

Jet substructure and probes of CP violation in Vh production

R. M. Godbole,^a D. J. Miller,^b K. A. Mohan^a and C. D. White^b

^a*Centre for High Energy Physics, Indian Institute of Science, Bangalore 560 012, India*

^b*School of Physics and Astronomy, Scottish Universities Physics Alliance, University of Glasgow, Glasgow G12 8QQ, Scotland, UK*

E-mail: rohini@cts.iisc.ernet.in, David.J.Miller@glasgow.ac.uk,
kirtimaan@cts.iisc.ernet.in, Christopher.White@glasgow.ac.uk

ABSTRACT: We analyse the hVV ($V = W, Z$) vertex in a model independent way using Vh production. To that end, we consider possible corrections to the Standard Model Higgs Lagrangian, in the form of higher dimensional operators which parametrise the effects of new physics. In our analysis, we pay special attention to linear observables that can be used to probe CP violation in the same. By considering the associated production of a Higgs boson with a vector boson (W or Z), we use jet substructure methods to define angular observables which are sensitive to new physics effects, including an asymmetry which is linearly sensitive to the presence of CP odd effects. We demonstrate how to use these observables to place bounds on the presence of higher dimensional operators, and quantify these statements using a log likelihood analysis. Our approach allows one to probe separately the hZZ and hWW vertices, involving arbitrary combinations of BSM operators, at the Large Hadron Collider.

Contents

1	Introduction	1
1.1	Higher Dimensional Operators	3
2	Event Simulation and Selection	5
2.1	Zh production	6
2.2	Wh production	7
2.3	Detector effects	7
2.4	Higher order effects	8
2.5	Reconstructing the neutrino momentum	8
2.6	Sensitivity to anomalous couplings	9
3	Angular observables	11
4	Multi-Variable Likelihood analysis	18
5	Asymmetries	25
6	Conclusion	28
A	Matrix elements for Vh production	29

1 Introduction

Both before and after the discovery of a new resonance at the Large Hadron Collider (LHC) [1, 2], much attention has been focused on how to efficiently determine its spin and couplings [3–43]. Deviations from Standard Model (SM) behaviour would signal the presence of new physics beyond the Standard Model (BSM), and there are significant motivations for expecting such deviations to be present at some level, not the least given that new physics is expected to explain or clarify the nature of electroweak symmetry breaking. There are two main approaches for addressing BSM corrections to the Higgs sector. The first is to postulate the existence of a specific theory, and analyse how the particle content leads to corrections to SM observables. This approach must necessarily be used for collider experiments whose energy exceeds the lowest energy scale associated with the new physics (e.g. a new particle mass). The second possibility is to use effective field theory techniques to write down possible corrections to the SM Lagrangian in the form of additional operators, which ultimately arise from integrating out the new degrees of freedom in a particular BSM model. One may systematically classify these operators according to their mass dimension, such that higher-dimensional ones are suppressed by increasing powers of the new physics scale. For a given mass dimension, there is a finite

set of possible independent operators. By including all of these (in a chosen basis), one allows for the most general corrections to the SM. This approach has the benefit of being completely model-independent, but at the price of being applicable only for energy scales which are below the lowest new physics scale. This is a reasonable assumption to make, given that current studies (such as those referred to above) appear to show only small deviations, if any, from the Standard Model.

In this paper, we focus on the coupling of the Higgs to vector bosons $V = W, Z$. The operators relevant for these interactions have been classified in [44–46]. It is important to understand that bounds derived on the hZZ vertex, do not automatically translate to bounds on the hWW vertex. For example, as argued in ref. [38], violation of custodial symmetry can arise naturally in new physics models. While higher dimension operators may be constrained from precision tests as well as Higgs rates [41, 47, 48], the constraints depend on various assumptions. Unambiguous and definitive constraints can only be determined by directly probing the nature of the hZZ and hWW vertices *separately*. In order to determine whether or not the higher dimension operators are present in nature, one must study various scattering processes that involve the hZZ and hWW vertices. The decay of the Higgs boson to Z boson pairs at the LHC has been studied in [13, 14, 16, 24, 49–54], which focused on the fully leptonic decay channel. Combined with LHC data, this disfavors the possibility that the recently discovered boson is purely pseudoscalar at $\sim 2 - 3\sigma$ significance [55–59]. The decay of the Higgs to W boson pairs is more difficult in principle, due to the limited kinematic resolution inherent in having missing energy in the final state. This mode has been investigated in [13, 15, 19, 21, 60, 61]. As ref. [15] in particular makes clear, the kinematic cuts used to select events in this case may overly diminish the signal for BSM effects.

Another possibility is to study the production of the Higgs boson via vector boson fusion, and angular observables exist for distinguishing various BSM scenarios [62–65]. However, a deficiency of this mode is that it is not possible to unambiguously separate BSM contributions to the hWW and hZZ vertices. Furthermore, ref. [26] argued that the momentum dependence associated with an anomalous hVV vertex can have a dramatic effect on the rapidities of the quarks that emit the vector bosons, and consequently of the acceptance of the event selection cuts.

Given the above difficulties, the possibility has been explored of using a future electron-positron collider, such as the proposed International Linear Collider (ILC) or equivalent [66–70]. The different BSM corrections have different CP properties, which manifest themselves in different angular decay products of the Higgs and associated particles. An e^+e^- collider can explore this in detail using polarised beams. In addition, the partonic centre of mass energy is known precisely in such a collider, and one may distinguish different contributions to the VVh vertices using the fact that they lead to different power-like growths of associated Higgs production cross-sections near threshold [66]. However, it is still not possible to unambiguously determine BSM corrections to the WWh and ZZh

vertices separately at such a collider ¹. Whilst this is possible at the LHeC (a proposed e^-p facility) [71, 72], it is clearly advantageous to use the LHC itself to achieve this.

In this paper, we show that one can indeed distinguish the presence of higher dimensional operators at the LHC, using the associated production of a Higgs with a vector boson (Vh production), where the Higgs boson decays to a pair of b quarks. For many years, it was thought to be impossible to analyse this mode, due to the presence of large QCD backgrounds. This situation has changed due to the development of jet substructure techniques, as pioneered in [73]. By requiring the Higgs boson to be boosted, the b quark pair from its decay will be approximately collinear. One may then distinguish the boosted Higgs signal by looking for a fat jet, containing two smaller subjets (modulo a filtering procedure) each of which reconstructs the b mass. Subsequently, a number of approaches for utilising jet substructure have been developed [74–78], together with analytic understanding [79, 80] and applications in experimental analyses [81–91]. As the present authors already pointed out in [27], reconstructing both the Higgs momentum and the associated vector boson opens up the use of polarisation-related methods for Vh production, analogous to those used in the e^+e^- studies mentioned above: the spin state of the associated vector boson is influenced by the presence of higher dimensional operators in the Higgs sector, so that angular observables involving the vector boson decay products can be used to constrain BSM physics. Furthermore, this can be done separately for the Zh and Wh channels, allowing one to independently elucidate the nature of the hZZ and hWW vertices.

The structure of our paper is as follows. Throughout the remainder of this introduction, we discuss the framework we are using for higher dimensional operators in more detail. In section 2, we describe the details of our simulations and the selection cuts. We also make a note of higher order effects in both Wh and Zh production and describe kinematic reconstruction issues. In section 2.6 we describe the increased sensitivity to non-SM couplings of the hVV vertex, mentioned earlier. In section 3 we construct and describe various angular observables that are able to discriminate the different non-SM couplings of the hVV vertex. In section 4 we construct likelihoods out of various observables and estimate the required luminosity for the 14 TeV LHC to constrain the anomalous hVV couplings. In section 5 we construct a CP-odd asymmetry that is linearly sensitive to the CP-odd coupling and hence to CP violating effects in the hVV vertex. Finally in section 6 we summarize and conclude.

1.1 Higher Dimensional Operators

As already mentioned in the introduction, one may encapsulate the structure of BSM physics in a model-independent way by adding higher dimensional operators to the SM Lagrangian. One starts by classifying all possible higher-dimensional operators that can

¹ It is not easy to study the anomalous WW couplings via the process $e^+e^- \rightarrow \nu\bar{\nu}h$ since there are large irreducible backgrounds to this process and a high degree of beam polarization as well as measurements of the polarization of the final states are required. See ref. [68] for details.

serve as corrections to the Standard Model Lagrangian and that are gauge-invariant, an exercise which was first carried out in [44, 92, 93]. There is a single dimension five operator which, after electroweak symmetry breaking, is responsible for neutrino masses and mixings. One is then motivated to proceed to dimension six operators, of which there are many - ref. [44] lists over a hundred. However, not all of these are independent, as one may use equations of motion to relate them. To this end, ref. [46] showed that there are 59 independent operators. Reference [45] expressed these in a basis more directly suited to Higgs boson physics, and also discussed how the coefficients of these operators scale differently if electroweak symmetry breaking is weakly or strongly coupled. Effective operators for a hypothetical spin one or spin two Higgs boson have been presented in [94], which also discusses their implementation in a computational framework inclusive of next-to-leading order matrix element corrections and parton shower effects. A pedagogical review of the literature may be found in section 2 of ref. [95].

Since our objective is to study the Lorentz structure of the hVV vertex for massive gauge bosons, we will only concern ourselves with a subset of the operators. It is sufficient to consider the following three operators ²

$$\begin{aligned}\mathcal{O}_{WW} &= \frac{g_2^2}{4\Lambda^2} \Phi^\dagger \Phi W_{\mu\nu}^i W^{i\mu\nu} , & \tilde{\mathcal{O}}_{WW} &= \frac{g_2^2}{4\Lambda^2} \Phi^\dagger \Phi W_{\mu\nu}^i \tilde{W}^{i\mu\nu} , \\ \mathcal{O}_{hW} &= \frac{ig_2}{\Lambda^2} b_{hW} (D^\nu W_{\mu\nu})^k \left(\Phi^\dagger \sigma^k \overleftrightarrow{D}^\mu \Phi \right) .\end{aligned}$$

Here Λ is the scale of new physics and the multiplicative Wilson coefficients b_{WW} , c_{WW} and b_{hW} parametrize the relative strengths of these operators. Writing the coupling in the form $i\Gamma^{\mu\nu}(k_1, k_2)\epsilon_\mu(k_1)\epsilon_\nu^*(k_2)$, where $\{\epsilon_\mu(k_i)\}$ ($i = 1, 2$) are the polarization vectors of the two gauge bosons, the HVV vertices one obtains are

$$\begin{aligned}i\Gamma_{hWW}^{\mu\nu}(k_1, k_2) &= i(g_2 m_W) \left[\eta^{\mu\nu} \left(1 + a_W - \frac{b_{W1}}{m_W^2} (k_1 \cdot k_2) + \frac{b_{W2}}{m_W^2} (k_1^2 + k_2^2) \right) \right. \\ &\quad + \frac{b_{W1}}{m_W^2} k_1^\nu k_2^\mu - \frac{b_{W2}}{m_W^2} (k_1^\mu k_1^\nu + k_2^\mu k_2^\nu) \\ &\quad \left. + \frac{c_W}{m_W^2} \epsilon^{\mu\nu\rho\sigma} k_{1\rho} k_{2\sigma} \right] ;\end{aligned}\tag{1.1}$$

$$\begin{aligned}i\Gamma_{hZZ}^{\mu\nu}(k_1, k_2) &= i \left(\frac{g_2 m_Z}{\cos \theta_w} \right) \left[\eta^{\mu\nu} \left(1 + a_Z - \frac{b_{Z1}}{m_Z^2} (k_1 \cdot k_2) + \frac{b_{Z2}}{m_Z^2} (k_1^2 + k_2^2) \right) \right. \\ &\quad + \frac{b_{Z1}}{m_Z^2} k_1^\nu k_2^\mu - \frac{b_{Z2}}{m_Z^2} (k_1^\mu k_1^\nu + k_2^\mu k_2^\nu) \\ &\quad \left. + \frac{c_Z}{m_Z^2} \epsilon^{\mu\nu\rho\sigma} k_{1\rho} k_{2\sigma} \right] ,\end{aligned}\tag{1.2}$$

²These correspond to the operators $\mathcal{O}_{\Phi W}$, $\mathcal{O}_{\Phi \tilde{W}}$ and \mathcal{O}'_{DW} in ref. [37].

where we have introduced the rescaled parameters

$$\begin{aligned} b_{W1} &= \frac{2 m_W^2 b_{WW}}{\Lambda^2}, & b_{W2} &= \frac{2 m_W^2 b_{hW}}{\Lambda^2}, \\ c_W &= \frac{2 m_W^2 c_{WW}}{\Lambda^2}, \end{aligned} \quad (1.3)$$

$$\begin{aligned} b_{Z1} &= \frac{2 \cos^2 \theta_w m_W^2 b_{WW}}{\Lambda^2}, & b_{Z2} &= \frac{2 m_W^2 b_{hW}}{\Lambda^2}, \\ c_Z &= \frac{2 \cos^2 \theta_w m_W^2 c_{WW}}{\Lambda^2}, \end{aligned} \quad (1.4)$$

and also rescaled the $\eta^{\mu\nu}$ contribution by a factor $1 + a_V$ in each case, to allow for full generality (i.e. sensitivity to rescalings of the Standard Model contribution). Note that while the terms in the first two lines of each of eqs. (1.1, 1.2) are CP-even, the terms in the third lines are CP-odd. Terms which are not proportional to $\eta^{\mu\nu}$ may be generated within the SM at higher orders of perturbation theory, although the resulting couplings are likely to be very small. Significantly large values of these couplings would be a signal for BSM physics.

One should note that, since we will always consider this vertex in processes where the V bosons are connected to external fermions, the terms $(b_{W2} (k_1^\mu k_1^\nu + k_2^\mu k_2^\nu))$ and $(b_{Z2} (k_1^\mu k_1^\nu + k_2^\mu k_2^\nu))$ vanish due to current conservation and we will not consider them any further. Note that the extra factors of $\cos \theta_w$ in (b_{Z1}, c_Z) as compared to (b_{W1}, c_W) signal violation of custodial symmetry. These factors disappear when the corresponding \mathcal{O}_{BB} , $\tilde{\mathcal{O}}_{BB}$ and \mathcal{O}_{hB} operators are of equal strength.

The aim of this paper is to perform a detailed study of angular observables designed to distinguish the three contributions to each hVV vertex: SM, BSM CP even, and BSM CP odd, building upon the preliminary study of [27]. In what follows we will present results in terms of the vertex parameters appearing in eqs. (1.1) and (1.2), rather than the coefficients of the higher dimensional operators directly, in order to be more general. The choice of operators is not unique, and different choices will result in different translations between the two sets of parameters (eqs. (1.3) and (1.4)). We discuss the details of our analysis framework in the following section.

2 Event Simulation and Selection

We consider Vh production ($V = Z, W^\pm$), where the V decays leptonically, and the h boson to a $b\bar{b}$ pair. Further, we use jet substructure algorithm techniques to not just separate QCD backgrounds but use it to reconstruct the parton-parton CMS frame for Vh production. In this section we describe the tools and methods used for our analysis, including the selection cuts utilised for both Wh and Zh production. We simulate all processes using **MadGraph5** [96], having implemented the effective Lagrangian in **FeynRules** [97, 98].

The output is interfaced with `Pythia6` [99] for showering and hadronization. We use the ‘Z2Star’ tune for `Pythia6`, including initial and final state radiation along with effects of multiple interactions, and use the CTEQ6L1 parton distribution functions [100]. We use `FastJet` [101] to cluster jets. Note that cross-checks were carried out at the parton level using analytic expressions.

Our selection cuts for these signal processes are as follows.

2.1 Zh production

For Zh production we require:

1. A fat jet of radius $R = \sqrt{\Delta y^2 + \Delta \phi^2} = 1.2$ and transverse momentum $p_T > 200$ GeV. After applying the mass drop and filtering procedure of [73] on this fat jet, we require no more than three sub-jets with $p_T > 20$ GeV, $|\eta| < 2.5$, and radius $R_{sub} = \min(0.3, R_{bb})$, where R_{bb} is the separation of the two hardest subjets, both of which must be b -tagged. In addition, we also require that the invariant mass of this jet system reconstructs the Higgs mass in the range 110 - 140 GeV.
2. Exactly 2 leptons (transverse momentum $p_T > 20$ GeV, pseudo-rapidity $|\eta| < 2.5$) of same flavour and opposite charge, with invariant mass within 10 GeV of the Z mass m_Z . These should be isolated.
3. The reconstructed Z has a $p_T > 150$ GeV, with azimuthal angle satisfying $\Delta\phi(Z, h) > 1.2$.

The first selection requirement listed above is used to reconstruct the decaying Higgs. The requirement for a fat jet with large transverse momentum means that we are looking at events with a highly boosted Higgs. Note that by allowing for a third hard jet inside the fat jet, the procedure allows for an extra jet other than the two b -jets originating from the radiation of a gluon from the b -quarks. The second requirement allows for reconstruction of the Z boson, where the isolation criterion removes most of the $t\bar{t}$ and QCD background. The third requirement ensures that the Higgs and the Z boson lie in almost the same plane of production as is expected for the signal. Note that the above selection criteria are applied after simulating a detector response to be described in section 2.3.

After cuts, the only significant surviving background process is $Z + \text{jets}$. Cross-sections at Leading Order (LO) after cuts are shown in table 1. The $h \rightarrow b\bar{b}$ branching ratios were taken from Ref. [102]. The cross-sections for backgrounds, the SM, the pure CP-odd operator $c_V \neq 0$ and the two BSM CP-even operators $b_{V1} \neq 0$ and $b_{V2} \neq 0$ are shown, with all other couplings set to zero in each case. The values of the BSM couplings are chosen so as to reproduce the SM total cross-section, without any selection cuts. Note that in spite of this choice of couplings, the cross-sections after cuts for the BSM cases are much higher than the SM, implying a greater acceptance for the BSM cases. We will elaborate on this point later.

Channel	Vh_{SM}	V+jets	$t\bar{t}$	Single top	$b_{W1} = 0.2$	$c_W = 0.25$	$b_{W2} = 0.03$
$W^\pm h$	0.355	0.28	0.13	0.06	1.45	2.14	7.11
					$b_{Z1} = 0.23$	$c_Z = 0.30$	$b_{Z2} = 0.08$
Zh	0.12	0.23	0	0	0.48	0.73	2.22

Table 1. Cross-sections (fb) evaluated at leading order for the 14 TeV LHC after applying all cuts. V +jets corresponds to the Z +jets background for the Zh process and W +jets for the Wh process. For the last three columns the SM contribution was set to zero and each of the values of b_{V1}, b_{V2}, c_V were set to reproduce the SM total cross-section before applying cuts.

2.2 Wh production

For Wh production we require the following:

1. The Higgs reconstructed as above.
2. Exactly one hard lepton ($p_T > 30$ GeV, $|\eta| < 2.5$), isolated as above.
3. Missing transverse momentum $\cancel{p}_T > 30$ GeV.
4. The reconstructed W has $p_T > 150$ GeV and azimuthal angle satisfying $\Delta\phi(h, W) > 1.2$.
5. No additional jet activity with $p_T^{jet} > 30$ GeV, and rapidity $|y| < 3$ (to suppress single and top pair production backgrounds).

The difference between Zh and Wh is that in the latter case only the transverse momentum of the W boson can be determined in the detector. However, it is possible to some extent to reconstruct the neutrino momentum as will be discussed in what follows. The LO cross-section for the signal and major backgrounds are detailed in table 1. Once again, the choice of couplings (b_{W1}, b_{W2}, c_W) is such that the total cross-section (before any kinematic cuts) is identical to the SM total cross-section. As in the case of Zh , we see that in this case also, the cross-section after cuts is larger for the BSM couplings, indicating a higher acceptance of the selection cuts to BSM physics. In the following we describe certain detector effects that we have considered in our analysis.

2.3 Detector effects

While a full detector simulation is beyond the scope of this study, it is still important to check whether the inefficiencies of a detector do not dilute the effects that are observable with exact reconstruction. To this end we use the **Delphes 3** package [103] for a fast simulation of detector response. We set the parameters of the detector simulation tuned for the CMS detector, with some modifications:

- The lepton isolation radius R is set to a reduced value of 0.3, to allow for isolation of leptons in high transverse momentum events where the leptons will be collimated.

- We modify the jet reconstruction algorithm for the detection of a boosted Higgs as described above and set the b-tagging efficiency to be 0.6 while the mis-tagging efficiency for c-jets is 0.2 and for all other jets is 0.001.

We use the `Delphes` package since it has been shown to give good agreement with data [103]. However, we do not carry out any validation with experiment for our choice of parameters as this is beyond the scope of the discussion presented here.

2.4 Higher order effects

At LO and at NLO in QCD, Vh production occurs through quark-initiated processes. The NLO (QCD) correction to the LO order process is given entirely by corrections to the Drell-Yan process [104–106]. The NLO process produces extra QCD radiation in the initial state thus affecting observables such as the transverse momentum of the final state particles. It should be noted that such effects are large only near the threshold of the transverse momentum cuts due to collinear and/or soft initial state radiation [107]. In fact the use of asymmetric transverse momentum cuts on the V-boson ($p_T^V > 150$ GeV) and Higgs ($p_T^h > 200$ GeV) transverse momenta means that most of this effect will be concentrated in the region ($p_T^V < 200$ GeV). However, the contribution to the cross-section from this region of phase space is small and hence we neglect this effect.

The K-factor (ratio to the LO order cross-section) for NLO (QCD) is about 1.2, see for example ref. [107]. In the special kinematic region of the boosted analysis the K-factor for both Zh and Wh was found to be ~ 1.5 in Ref. [73]. For the $Zb\bar{b}$ background the K-factor was found to be about the same while for $Wb\bar{b}$ the K factor is higher and about 2.5. The other main background, $t\bar{t}$ production, was found to have a K-factor ~ 2 . We will use these values of the K-factor in our analysis of likelihoods in section 4.

Furthermore, we simulate the kinematics of an extra jet using the MLM matching procedure [108] with one additional jet for both signal and background. We have checked that our results do not vary significantly with the addition of this extra jet. For Wh production, since we veto events with additional hard jets to remove backgrounds, the effect of extra radiation on the observables we consider is negligible.

2.5 Reconstructing the neutrino momentum

One must reconstruct the neutrino in Wh production to determine our angular observables. We identify the neutrino transverse momentum $\mathbf{p}_{T,\nu}$ with the missing transverse momentum $\mathbf{\not{p}}_T$. As explained previously, the missing transverse momentum is approximated by taking the negative vector sum of the transverse momentum of all particles that can be detected (> 0.5 GeV). In order to evaluate the full four momentum of the neutrino, we demand that the squared sum of the neutrino and lepton momenta be equal to the squared W boson mass ($(p_\nu + p_{l_1})^2 = M_W^2$), and solve the resulting quadratic equation. Comparing with the “true” Monte-Carlo generated neutrino momentum, we find that choosing a given solution out of the two possible ones, reconstructs the true neutrino momentum 50% of

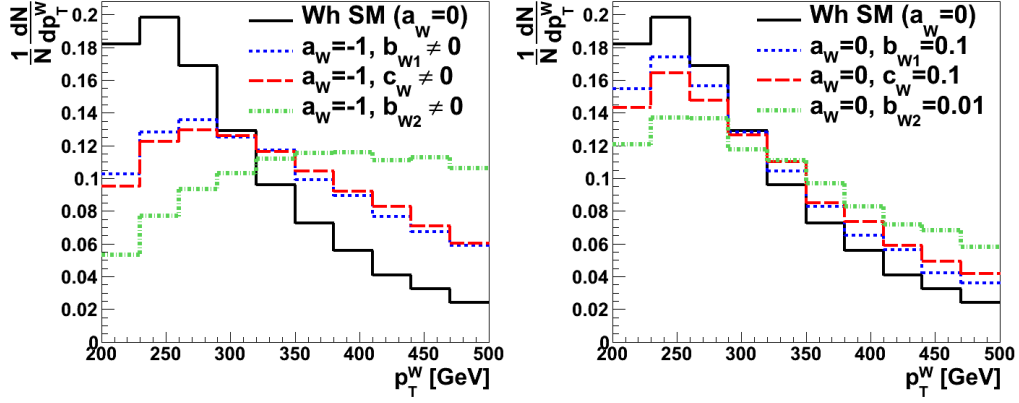


Figure 1. Plots showing the transverse momentum dependence of the W boson in Wh production after applying the selection cuts listed in section 2. **Left:** Pure SM or BSM (all other couplings zero); **Right:** Three cases of admixtures of the SM and BSM couplings (all other couplings set to zero).

the time, with $\simeq 5\%$ giving imaginary solutions. One may improve on this by comparing the boosts of the Higgs β_z^h and reconstructed W β_z^W in the z direction. The solution with the minimum value for $|\beta_z^W - \beta_z^h|$ gives the true neutrino momentum in 65% of cases. We thus present all our results using the latter algorithm.

2.6 Sensitivity to anomalous couplings

It has been observed that the momentum dependence of the BSM couplings of the hVV vertex push the p_T and invariant mass ($\sqrt{\hat{s}_{Vh}}$) distributions to larger values [25, 26, 109], due ultimately to the extra momentum factors present in the BSM vertices. This is confirmed in the distributions shown in the plots in figure 1. The plot on the left shows the transverse momentum distribution of the W boson in Wh production in the SM (black solid line) compared each of the pure BSM couplings (with the SM contribution set to zero), using the selection cuts described in the previous section. The values of the couplings have been chosen so that they reproduce the SM cross-section when no cuts are applied. We see that the effect of all the BSM couplings is to push the p_T^W distribution to larger values. The effect is even more pronounced for the coupling b_{W2} while the b_{W1} and c_W couplings have a strong but less pronounced effect on this distribution. In the right plot we show the same distribution but this time for admixtures of the SM coupling ($a_W = 0$) with each of the BSM couplings. The effect of the BSM couplings is still easily discernible, though less prominent than compared to the plot on the left. The larger p_T distributions of the Vh system also lead to larger Higgs boosts and a reduced separation R_{ll} and R_{bb} between the leptons (from the decay of the gauge bosons) and b jets (from the decay of the Higgs) respectively. As mentioned in the previous section, this effect is further quantified by the results of table 1, in which the cross-section for pure BSM processes after cuts is significantly higher than the SM result, after imposing that the cross-sections agree before

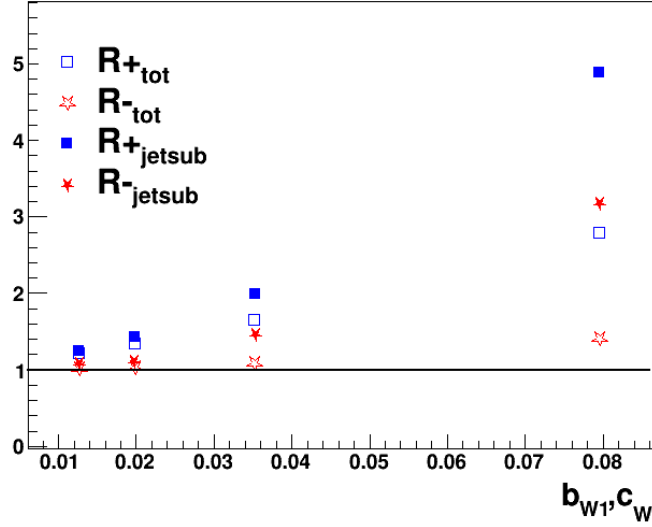


Figure 2. The ratio of the cross-sections R^- (mixture of SM and CP odd) (red stars) and R^+ (mixture of SM and the BSM CP even term) (blue boxes) both before (hollow markers) and after (bold markers) applying selection cuts for the Wh channel for 14 TeV LHC. The x -axis corresponds to the strength of each of the couplings b_{W1} or c_W .

cuts.

In figure 2, we consider the SM coupling $a_W = 0$ supplemented by either the c_W (CP-odd) coupling or the b_{W1} coupling applied to the Wh channel. We show the ratio of the SM+BSM and SM cross-sections both for the total cross-section ($R^{\pm}_{tot} = \sigma^{SM+BSM\pm}_{tot}/\sigma^{SM}_{tot}$) and the cross-section after applying selection cuts ($R^{\pm}_{jetsub} = \sigma^{SM+BSM\pm}_{jetsub}/\sigma^{SM}_{jetsub}$). Here R^+ and R^- correspond to the case ($a_W = 0, b_{W1} \neq 0$) and ($a_W = 0, c_W \neq 0$) respectively. As is expected, both ratios decrease with the strength of the BSM couplings and approach unity as the BSM couplings tend to zero. R^+_{tot} shows a faster rise with coupling strength than R^-_{tot} . This is because the interference term in the matrix element squared for the CP-odd coupling does not contribute to the cross-section³. Importantly, R_{jetsub} (for both couplings) increases at a faster rate than R_{tot} with increasing values of the corresponding couplings. Similar results also hold for the second CP-even anomalous coupling b_{W2} . These ratios are therefore quite sensitive to the presence of anomalous couplings. Whilst not directly experimentally measurable, they can be determined by comparing an experimental measurement of the Vh signal with a precise theoretical prediction for the SM only contribution. If this lies away from unity, this constitutes a strong indication of BSM physics. Another feature that should be noted is that the ratio of the ratios ($R^{\pm}_{jetsub}/R^{\pm}_{tot}$) increases at a faster rate for the CP-odd coupling than it does for the CP-even coupling.

³In practice, if the squared term is larger than the interference term, this is an indication that the effective theory framework is breaking down. Here, however, we are merely quantifying the effect by which selection cuts enhance BSM effects, by fixing the BSM cross-section to be artificially high (equivalent to an unphysically low cut-off scale).

This is in agreement with the results of table 1, where it was observed that the acceptance to the selection cuts of the pseudo-scalar state was higher than a scalar with anomalous coupling b_{W2} .

3 Angular observables

In this section, we consider differential observables that can distinguish between the different BSM vertices occurring in the hVV interaction. One such observable, the transverse mass of the Vh system, has been used at the Tevatron to probe the hWW vertex [110], however, it has been shown to be ineffective at the LHC [25]. Furthermore, the CP-odd coupling contributes to this observable only through quadratic terms in the matrix element squared and therefore is not the most sensitive observable⁴. Angular observables, as we will show, can be *linearly* sensitive to the anomalous couplings. This is useful in that one may construct asymmetry parameters that are manifestly zero for the SM, such that any non-zero measurement constitutes discovery of new physics. Note that in the context of effective theory analysis, constructing observables that are linear in the anomalous couplings is of paramount importance.

The tensor structure of the BSM vertices will be reflected in the angular distribution of the decay products of the gauge boson⁵. To this end, we construct various angular observables that could discriminate between the different vertex structures. The momenta of the V and Higgs bosons are reconstructed from the leptons and jets as follows:

$$p_V = p_{l_1} + p_{l_2}, \quad p_h = p_{b_1} + p_{b_2} + p_j, \quad (3.1)$$

where $\{p_{b_i}\}$ are the momenta of the b jets, p_j is the momentum of the third jet if it is reconstructed and p_{l_1} and p_{l_2} are the momenta of the lepton and the anti-lepton respectively (for Wh , p_{l_1} corresponds to the lepton momentum and p_{l_2} to the neutrino). With these momenta, we may define

$$\cos \theta^* = \frac{\mathbf{p}_{l_1}^{(V)} \cdot \mathbf{p}_V}{|\mathbf{p}_{l_1}^{(V)}| |\mathbf{p}_V|}, \quad (3.2)$$

Here $\mathbf{p}_X^{(Y)}$ corresponds to the three momentum of the particle X in the rest frame of the particle Y . If Y is not specified then the momentum is defined in the lab frame. The parameter $\cos \theta^*$ corresponds to the angle between the direction of the decaying lepton in the rest frame of the V boson with the direction of flight of the V boson in the lab frame. This angle, first defined in [66], encodes the W boson polarization.

⁴Care must be taken if such quadratic terms become important, as this signals a potential breakdown of the effective theory description.

⁵Note, the Higgs has spin zero; angular distributions of its decay products are uncorrelated from production and hence do not carry any information about the hVV vertex in Vh production. Angular correlations of the decay products of the Higgs would reflect the properties of the decay vertex and not the production vertex; as in $h \rightarrow V^{(*)}V^{(*)}$ decays.

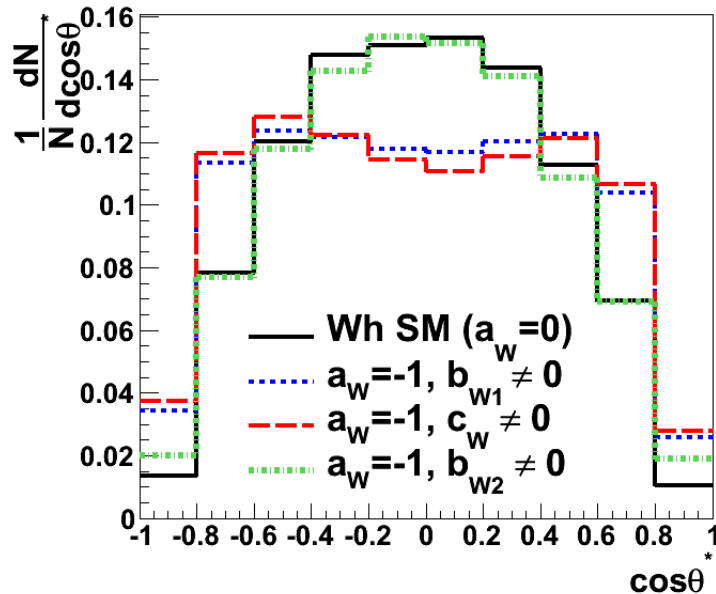


Figure 3. Plot of the distribution of the angle $\cos\theta^*$ for W^+h production, for pure SM and BSM operators. The values of the couplings are chosen as in table 1, so as to reproduce the SM cross-section (before cuts).

The SM and BSM couplings lead to mostly longitudinal and transverse W bosons respectively. That $\cos\theta^*$ then effectively distinguishes SM and BSM effects can be seen in figure 3. We see that the SM distribution (black solid line) peaks at $\cos\theta^* = 0$ and vanishes at $\cos\theta^* = \pm 1$. The distribution for the BSM coupling b_{W2} (green dot-dashed line) closely follows the SM distribution. This is expected since the tensor structure of the vertex in both these cases is the same. In contrast, the couplings b_{W1} and c_W produce distributions that have minima at $\cos\theta^* = 0$. They too appear to vanish at $\cos\theta^* = \pm 1$, however this is the effect of the selection cuts⁶. Without applying any selection cuts the distribution for these two cases peak at $\cos\theta^* = \pm 1$.

The behaviour of this distribution for each of the couplings can be understood as follows. For a transversely polarized W boson, the decay lepton spins align themselves perpendicular to the direction of motion of the W boson and gives rise to a distribution of the form $(1 \pm \cos\theta^*)^2$, while in the case of a longitudinally polarized W boson, the spins of the decay leptons align themselves along the direction of the W boson and give rise to a distribution of the form $\sin^2\theta^*$. The two BSM couplings b_{W1} and c_W produce more transversely polarized W boson states while the SM coupling and the coupling b_{W2} produce more longitudinally polarized W bosons. Using this distribution, it is therefore possible to differentiate between vertex structures with couplings b_{W1} or c_W from the vertex structure with couplings a_W or b_{W2} , but not between b_{W1} and c_W or between a_W and b_{W2} .

⁶All the selection cuts deplete this region of phase space, with strongest effects coming from the transverse momentum and rapidity cuts of the lepton.

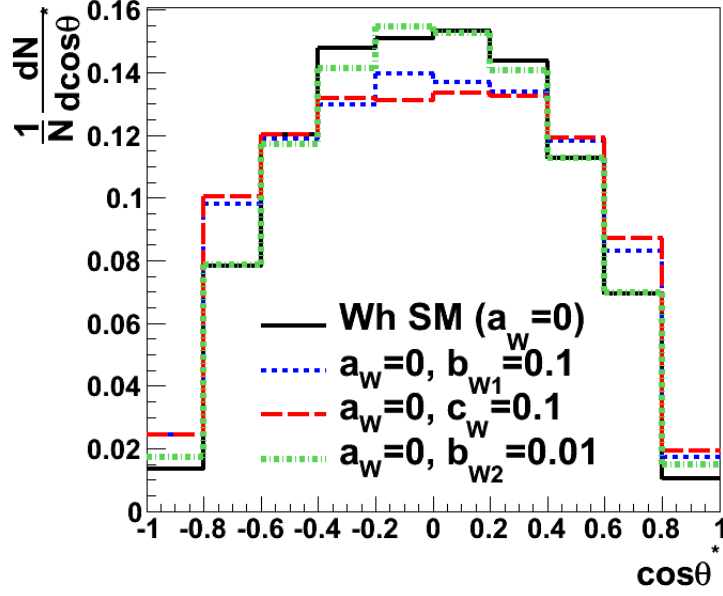


Figure 4. Plot of the distribution of the angle $\cos \theta^*$ for W^+h production, for admixtures of SM and BSM couplings.

In figure 4 we present plots of the same observable $\cos \theta^*$ for admixtures of the SM coupling with each of the BSM couplings. We present three cases corresponding to $(a_W = 0, b_{W1} = 0.1)$, $(a_W = 0, c_W = 0.1)$ and $(a_W = 0, b_{W2} = 0.01)$. We see that differences, though reduced, are still discernible in this distribution. Similar results also hold for Zh production.

To fully distinguish the CP even (b_{W1}) and odd (c_W) BSM contributions, one must construct CP-odd observables, which is difficult in principle for a proton–proton collider [111]. For Zh production, Ref. [112] considered two such observables, although these are sensitive to radiation and hadronization corrections; Ref. [113] defined observables which are insensitive to the CP nature of BSM contributions. Ref. [49] examined CP-odd asymmetries in Wh production with the decay $h \rightarrow W^{(*)}W^*$, though the effect of the BSM CP even term was not considered. The hint for possible CP-odd observables comes from looking at the matrix element squared for the process $q(k_1)\bar{q}'(k_2) \rightarrow W^+(p_W)h(p_h) \rightarrow l^+(p_1)\bar{\nu}_l(p_2)h(p_h)$ shown in appendix A. The interference term between the CP-odd coupling and the SM coupling ($a_W c_W$), is proportional to $\epsilon_{\mu\nu\rho\sigma} k^\mu (p_h - k_1)^\nu p_W^\rho p_1^\sigma$, where $k = k_1 + k_2$ and $\epsilon_{\mu\nu\rho\sigma}$ is the anti-symmetric Levi-Civita tensor. Such a term depends on the angle between the plane of production of the Wh and the direction of flight of the lepton. This is depicted in figure 5.

We now construct the following angles based on the observation made above.

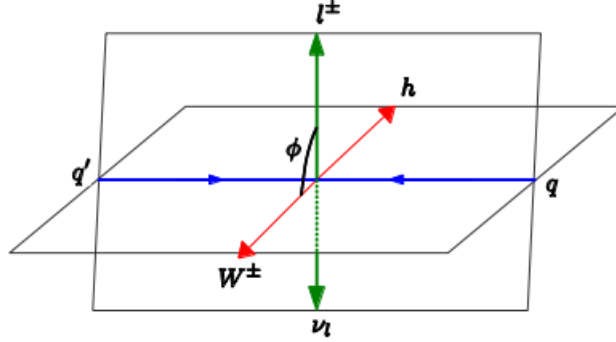


Figure 5. The angle (ϕ) between the plane of production and the lepton from the decay of the W boson.

$$\cos \delta^+ = \frac{\mathbf{p}_{l_1}^{(V)} \cdot (\mathbf{p}_h \times \mathbf{p}_V)}{|\mathbf{p}_{l_1}^{(V)}| |\mathbf{p}_h \times \mathbf{p}_V|}, \quad \cos \delta^- = \frac{(\mathbf{p}_{l_1}^{(h-)} \times \mathbf{p}_{l_2}^{(h-)}) \cdot \mathbf{p}_V}{|(\mathbf{p}_{l_1}^{(h-)} \times \mathbf{p}_{l_2}^{(h-)})| |\mathbf{p}_V|}, \quad (3.3)$$

$$\Delta\phi^{IV} = \Delta\phi(\mathbf{p}_{l_1}^{(V)}, \mathbf{p}_V). \quad (3.4)$$

We use the same notation for the momenta as described below eq. (3.2). For an e^+e^- collider where the direction (as well as the energy) of the lepton and anti-lepton are well known, it is sufficient to define the normal to the plane of production with the cross-product between any one of the leptons and the direction of flight of the Higgs or gauge boson. Note that the choice of vectors in e^+e^- collisions completely fixes whether the normal points ‘below’ or ‘above’ the plane of production. At the LHC, the information about the direction of the quark or anti-quark is not known and hence it is difficult to fix the direction of the normal to the plane of production. However, it is known that the valence quarks are likely to carry a larger fraction of the proton momentum. The direction of the normal to the plane of production can then be fixed by the momenta of the V and Higgs bosons. We use this fact to construct the first angle in eq. (3.4), $\cos \delta^+$, which corresponds to the angle between the direction of flight of the lepton (with the momentum evaluated in the rest frame of the V boson) and the plane formed by the V boson and the Higgs. In an e^+e^- collider, where the centre-of-mass and lab frames coincide, the gauge and Higgs bosons will be produced back to back. However, at the LHC one can take advantage of the asymmetric collision energies of the partons which results in the difference between the centre-of-mass and lab frame. For asymmetric collisions, the plane defined by the cross-product between the V boson and Higgs directions, coincides with the plane of production. In figure 6 we show the distribution of this observable for SM as well as for the anomalous couplings. In the plot on the left, the SM prediction is compared to the prediction for each of the

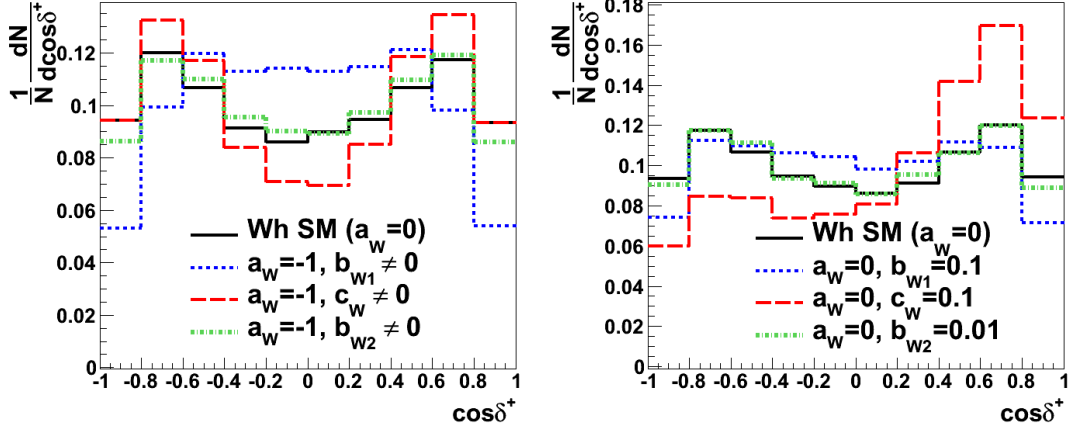


Figure 6. Plots showing the distribution of the angle $\cos \delta^+$ defined in eq. (3.4). **Left:** Pure SM and BSM couplings, chosen as in table 1, so as to reproduce the SM cross-section (before cuts). **Right:** Various admixtures of SM and BSM operators, with all other couplings set to zero.

anomalous couplings : $b_{W1} \neq 0$ (blue dotted line), b_{W2} (green dot-dashed) and c_W (red dashed) with all other couplings set to zero in each case. All distributions show a dip at $\cos \delta^+ = 0$. This is created by the transverse momentum cut on the leptons, since low p_T leptons will always be perpendicular to the normal to the plane of production.

We see from this distribution that for $b_{W1} \neq 0$ leptons are produced mostly in the plane of production, while for $c_W \neq 0$ the leptons tend to be produced mostly perpendicular to the plane of production. For two cases, the SM and for $b_{W2} \neq 0$, the distribution is flat (without cuts) and has a slight dip at $\cos \delta^+ = 0$ due to the p_T cuts, as explained above. This observable clearly discriminates between the $b_{W1} \neq 0$ and $c_W \neq 0$ cases, a feature that was absent in the distributions of observables discussed earlier.

More interesting effects can be seen in this observable when we consider admixtures of each of the anomalous couplings with the SM. In the right plot of figure 6 the distribution of three cases are compared with the SM expectation: ($a_W = 0, b_{W1} = 0.1$) (blue dotted line), ($a_W = 0, b_{W2} = 0.01$) (green dot-dashed) and ($a_W = 0, c_W = 0.1$) (red dashed), with all other couplings set to zero in each case. As expected, the distribution for the case ($a_W = 0, b_{W2} = 0.01$) follows the SM distribution closely. The CP-even ($a_W = 0, b_{W1} = 0.1$) case is similar to the pure anomalous coupling case ($a_W = -1, b_{W1} \neq 0$). We have checked that the interference term alone for the case ($a_W = 0, b_{W1} = 0.1$) produces a similar distribution to the case ($a_W = -1, b_{W1} \neq 0$) and is therefore linearly sensitive to b_{W1} . For the CP violating case ($a_W = 0, c_W = 0.1$) the distribution is skewed towards positive values of $\cos \delta^+$. This is due to the presence of the Levi-Civita tensor in the interference term of the matrix element squared as described above. Note that the distribution will peak for negative values of $\cos \delta^+$ if the sign of the coupling c_W were changed. This observable is therefore, linearly sensitive to c_W and hence to its sign. We will use this fact to construct asymmetries in the next section.

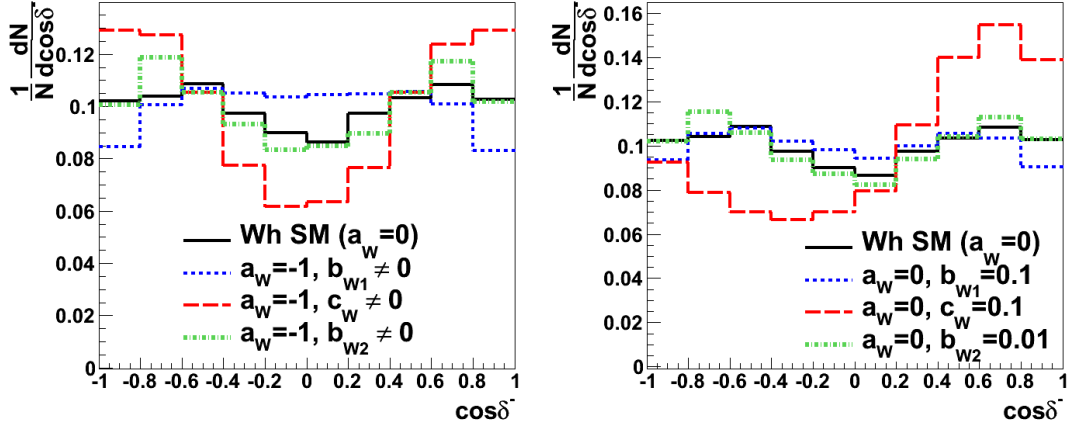


Figure 7. Plots showing the distribution of the angle $\cos \delta^-$ defined in eq. (3.4). **Left:** Pure SM and BSM couplings, chosen as in table 1, so as to reproduce the SM cross-section (before cuts). **Right:** Various admixtures of SM and BSM couplings, with all other couplings set to zero.

The second observable we consider is slightly more complicated in construction. The momenta of the two leptons from the decay of the gauge boson are evaluated in the frame in which the Higgs would be at rest, were its three momentum reversed⁷. Then $\cos \delta^-$ is the angle between the plane formed by the two leptons in this frame and the V boson in the lab frame. This angle is related to the angle ϕ depicted in figure 5. The distribution of this observable for SM is compared with three other cases in the left plot of figure 7: $b_{W1} \neq 0$ (blue dotted line), $b_{W2} \neq 0$ (green dot-dashed) and $c_W \neq 0$ (red dashed) with all other couplings set to zero in each case. The right plot of figure 7 compares the distribution of the SM expectation with admixtures of the SM couplings and the BSM coupling as given in the figure (and other couplings set to zero). The behaviour of this angle is very similar to that of $\cos \delta^+$. There are two noticeable differences. Firstly in the case $c_W \neq 0$ the distribution of $\cos \delta^-$ appears to show a more heightened difference from SM as compared to the distribution for $\cos \delta^+$. For the case when $b_{W1} \neq 0$ the opposite is true and $\cos \delta^+$ appears to show a greater difference from the SM distribution. This is also true when we set $(a_W = 0, b_{W1} = 0.1)$. For the CP-violating case, the same skewed behaviour of the distribution that was observed for $\cos \delta^+$, reappears here. As usual the distribution for the coupling b_{W2} in both the pure and mixed cases of the left and right plots of figure 7, follow closely the SM expectation.

The last observable we consider ($\Delta\phi^{IV}$) is the azimuthal angle difference of the lepton momenta (evaluated in the rest frame of the V boson) and the V boson momentum. The distribution for this observable is shown in figure 8. The left plot compares the SM expectation with three cases of the pure BSM couplings. The right plot compares the SM

⁷If the four momentum of the Higgs is written as (E_h, \mathbf{p}_h) , then this is the frame defined by the boost such that $(E_h, -\mathbf{p}_h) \rightarrow (m_h, 0)$

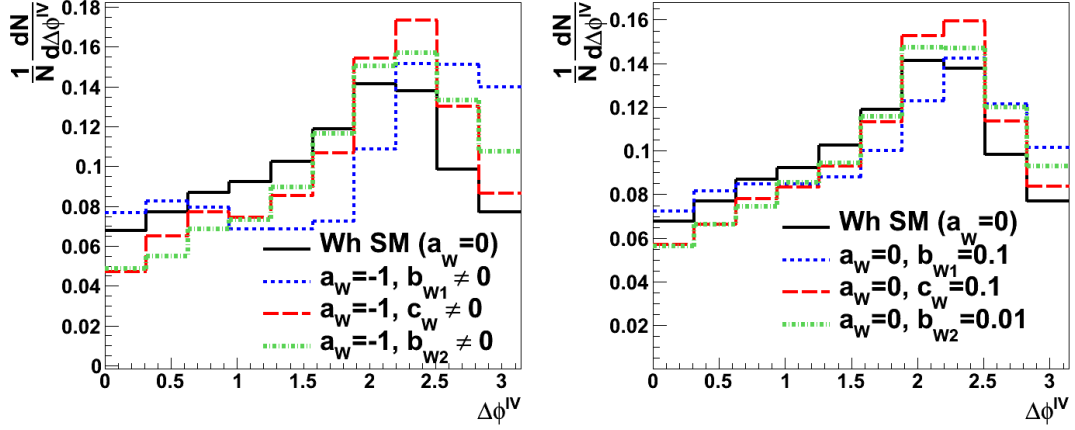


Figure 8. Plots showing the distribution of the angle $\Delta\phi^{IV}$ defined in eq. (3.4). **Left:** Pure SM and BSM couplings, chosen as in table 1, so as to reproduce the SM cross-section (before cuts). **Right:** Various admixtures of SM and BSM couplings, with all other couplings set to zero.

prediction with admixtures of SM with each of the BSM couplings. For all the cases we consider, there is a significant difference from the SM distribution of this observable. The most striking difference, however, is for the pure CP-even case ($b_{W1} \neq 0$) which displays a minimum in this distribution at $\Delta\phi^{IV}$ unlike the other cases. Differences between the distributions remain, although reduced, when considering admixtures of the SM coupling ($a_W = 0$) with each of the BSM couplings.

We also show in figure 9 distributions of the observables described above for the backgrounds to Wh production listed in table 1. The distribution of the various angles follow the SM distribution except for the angles $\Delta\phi^{IV}$ and $\cos\theta^*$. For completeness, we also show the distributions of the various angles defined in eq. (3.2) and eq. (3.4) for Zh production. In figure 10, the SM distribution (black solid line) is compared with the predictions of the three different BSM couplings. The values of the couplings are chosen as in table 1, so as to reproduce the SM total cross-section (before cuts). The distributions display a similar behaviour as compared to the analogous distributions in Wh production.

In figure 11, the SM distribution (black solid line) is compared with three cases which involve admixtures of the SM and BSM couplings. The asymmetries in the distributions of $\cos\delta^+$ and $\cos\delta^-$ that one observes in Wh production for the CP-violating case ($a_Z = 1, c_Z = 0.1$), although present, are far less prominent in Zh production. The reason for this difference can be ascertained by looking at the CP violating term in the matrix element squared. For Wh production, as described earlier, this term was simply proportional to a Levi-Civita tensor of the form $\epsilon_{\mu\nu\rho\sigma} k^\mu (p_h - k_1)^\nu p_W^\rho p_1^\sigma$. The CP violating term in the matrix element squared for Zh production has several instances of the Levi-Civita tensor that come with opposite signs. These do not cancel out (as they do in Wh production) since they are multiplied by axial and vector couplings (which are of different strengths). As a result, the distributions of $\cos\delta^+$ and $\cos\delta^-$ receive contributions from

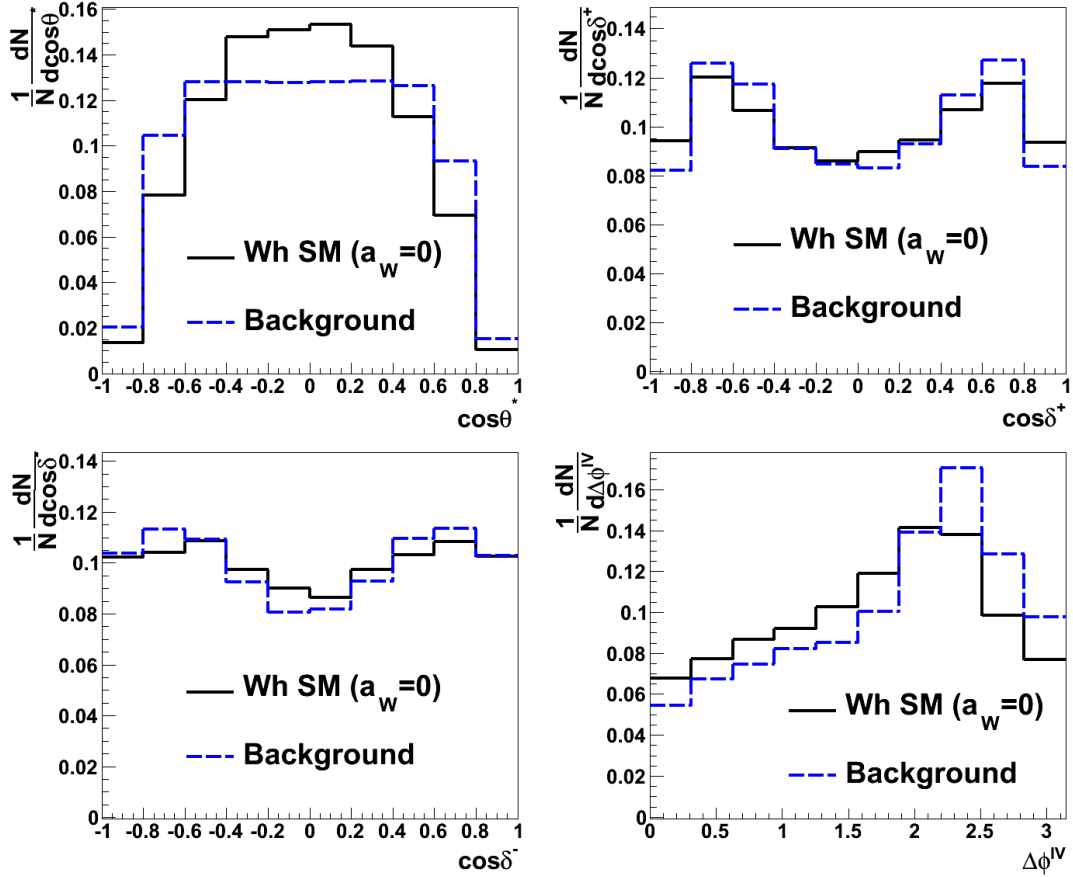


Figure 9. Normalized distribution of the observables defined in eq. (3.2) and eq. (3.4) for the backgrounds (blue dashed) to Wh production listed in table 1 and SM predictions (black solid lines).

Levi-Civita tensors of opposite sign and hence display a reduced skewness in distribution in comparison to the analogous distribution in Wh production.

We now have a set of observables that can discriminate not only the SM coupling from BSM couplings but also *between* the various BSM couplings, as evidenced by the distributions presented in this section. In order to fully assess the discriminating power of these observables and to estimate the typical luminosities that one would require at a 14 TeV LHC to rule out the various anomalous couplings, we perform a multi-variable likelihood analysis in the next section.

4 Multi-Variable Likelihood analysis

In the previous section we described the various observables that one could use in order to probe anomalous couplings in Vh production. We found that the transverse momentum of the V boson (or the Higgs), the angle $\cos\theta^*$ and any one of the correlated observables defined in eq. (3.4) can be used for this purpose. It is well known that the maximized

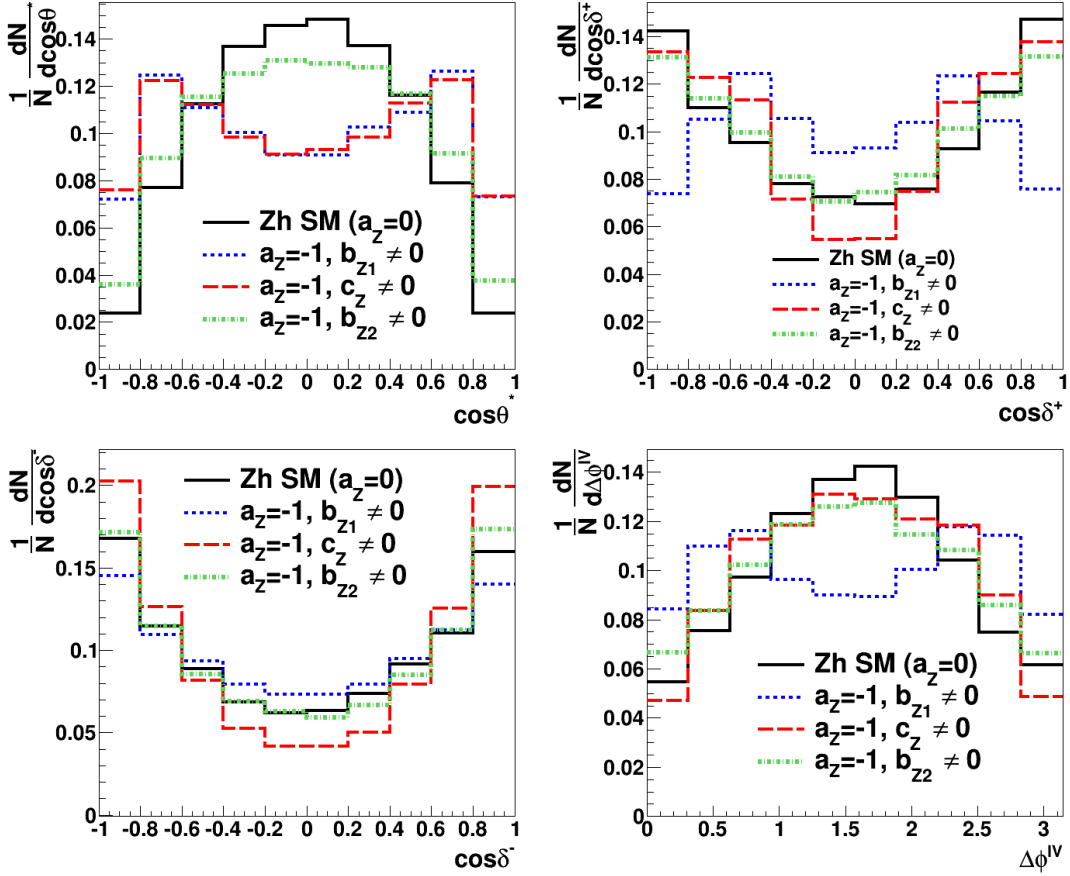


Figure 10. Normalized distribution of the observables defined in eq. (3.2) and eq. (3.4) for Zh production. The SM distribution (black solid line) is compared with the predictions of the three different BSM couplings: ($a_Z = -1, b_{Z1} \neq 0$) (blue dotted line) with all other couplings set to zero, ($a_Z = -1, b_{Z2} \neq 0$) (green dot-dashed) with all other couplings set to zero and ($a_Z = -1, c_Z \neq 0$) (red dashed) with all other couplings set to zero. The values of the couplings are chosen as in table 1, so as to reproduce the SM cross-section (before cuts).

log likelihood ratio provides the strongest test statistic according to the Neyman-Pearson lemma. Therefore in order to assess the sensitivity of these observables to probe anomalous couplings at the LHC, we perform a three dimensional extended binned-likelihood analysis. The procedure we follow is outlined below.

We set the SM expectation ($a_W = 0$) plus backgrounds as our null hypothesis. The alternate hypotheses are chosen to be the various cases which involve any one of the BSM couplings along with backgrounds. We define our likelihood as functions of a set of three observables. These are p_T^W , $\cos\theta^*$ and any one of the observables defined in eq. (3.4). In fact, we perform this analysis for three different definitions of the likelihood (L) which depend on the choice of observable, namely $L(p_T^W, \cos\theta^*, \cos\delta^+)$, $L(p_T^W, \cos\theta^*, \cos\delta^-)$ and $L(p_T^W, \cos\theta^*, \Delta\phi^{IV})$. As a first step we produce three dimensional histograms with the various combination of observables listed above. The choice of range and bins for each

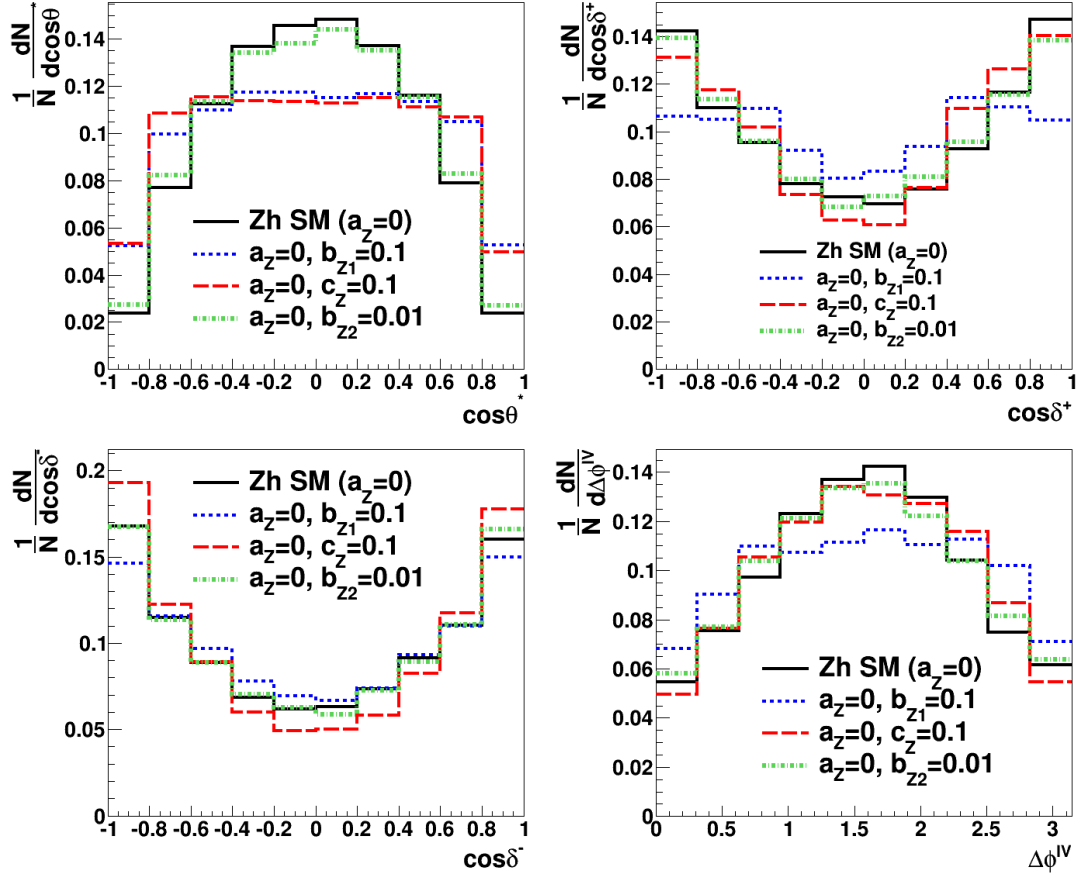


Figure 11. Normalized distribution of the observables defined in eq. (3.2) and eq. (3.4) for the Zh production. Various admixtures of SM and BSM operators are shown, with all other couplings set to zero.

of the observables is listed below.

- p_T^W : range (200, 1000) GeV, 10 bins
- $\cos \theta^*$: range $(-1, 1)$, 10 bins
- $\cos \delta^-$: range $(-1, 1)$, 10 bins
- $\Delta \phi^{lV}$: range $(0, \pi)$, 10 bins

The histograms are binned with at least 10^4 events after applying all selection cuts.

Using these histograms we can now determine the Likelihood function. Let t_i be the expected bin height (or number of events) of the i^{th} bin derived from theory (in our case from Monte Carlo simulations). The probability that the i^{th} bin will have n_i observed events (observed bin height) is a Poissonian probability given by

$$\frac{t_i^{n_i} e^{-t_i}}{n_i!}. \quad (4.1)$$

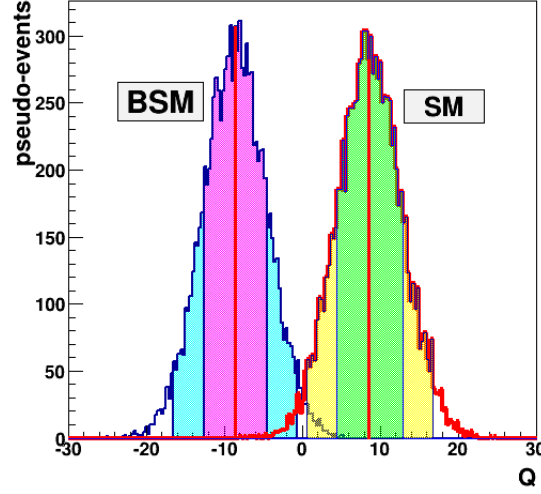


Figure 12. The distribution of \mathcal{Q} from the generation of 1×10^3 pseudo-events. For two hypotheses $X=SM$ (right curve) and $X=CP\text{-odd}$ (left curve).

We can now proceed to determine the probability of generating the full distribution for all of the histogram bins by multiplying the probability for each of the bins. The binned likelihood is then given by a Poisson distribution

$$L_X = \prod_i^N \frac{t_i^{n_i} e^{-t_i}}{n_i!}. \quad (4.2)$$

Here N is the number of bins, t_i is the expected number of events under the hypothesis X and n_i is the number of observed events. The likelihood ratio is then defined as

$$\mathcal{Q} = -2 \text{Log} \left(\frac{L(X|data)}{L(SM|data)} \right). \quad (4.3)$$

We now use these three dimensional histograms to generate “pseudo-data”. This is done by using the theoretically determined t_i to generate Poisson distributed random numbers which correspond to our pseudo-data. We repeat this procedure for all bins in order to generate pseudo-data. We then determine the distribution of the likelihood ratio \mathcal{Q} by generating 5×10^3 “pseudo-events”. A typical distribution for \mathcal{Q} is shown in figure 12.

Using the distribution \mathcal{Q} , we can determine the p-value of excluding the alternate (BSM hypothesis)⁸. We include the effects of backgrounds completely but only profile over the various nuisance parameters that arise from detector effects and selection cuts.

The results of this procedure are shown in figure 13 for the pure BSM cases, where we show the variation of the p-value of the BSM hypothesis against the luminosity. To assess

⁸We use the median value of the null hypothesis to determine the p-value of the alternate hypothesis. This corresponds to twice the p-value in the CL_s method used in LEP.

the sensitivity of each of the observables, we set the coupling strengths to values so that they reproduce the SM cross-section after applying all the cuts, i.e. ($a_W = -1, b_{W1} = 0.1$), ($a_W = -1, c_W = 0.1$) and ($a_W = -1, b_{W2} = 0.007$) with all other couplings set to zero for each of these cases. This choice of couplings hence eliminates the rate information from the analysis. We stress that this is done to check the discriminating power of the observables under consideration. The horizontal line indicates exclusion of the alternate hypothesis at 95% confidence level. A second horizontal line is shown in some cases below the first one and this indicates exclusion of the alternate hypothesis at 3σ confidence level. For two of the couplings c_W and b_{W1} we observe that the likelihood constructed with the $\Delta\phi^{lV}$ observable provides a slightly stronger discriminant. In both cases we find that exclusion of the pure BSM hypothesis at 95% confidence level is possible with $\sim 50\text{fb}^{-1}$ luminosity. The coupling b_{W2} can be excluded with even less data with exclusion 95% confidence level possible with just 30fb^{-1} luminosity. All the likelihoods produce similar results in this case. This is as expected since, the strongest discriminator for this coupling is the transverse momentum distribution, while angular observables for b_{W2} are not very different from SM predictions. An important point to note is that we have set the couplings to very small values. This does not correctly reproduce the Higgs partial decay widths. For example, if the Higgs were a pseudo-scalar, then in order to reproduce the SM decay width in $h \rightarrow V^{(*)}V^{(*)}$ decays, the coupling c_V should have a value ~ 3 . For such a large value of the coupling, the Vh production channel can easily rule out the pseudo-scalar hypothesis with $\sim 20\text{fb}^{-1}$ of data. We would like to emphasize that although a pure pseudoscalar hypothesis has been ruled out by an analysis of the Higgs decaying to four lepton channel, the same is not true for the hWW coupling [52]⁹. Since it is not easy to reconstruct the kinematics of the final state in the case of higgs decaying through W bosons, what we suggest is that it is possible to use only the rate information from the decay coupled with an analysis of Wh production (as prescribed here) to easily rule out the pure pseudoscalar hypothesis for the hWW coupling with a relatively small amount of luminosity.

We are, however, more interested in the case where there are admixtures of the SM coupling and the BSM couplings. In figure 14 we show the variation of the p-value for the alternate hypothesis with luminosity for 14 TeV LHC. For the case when ($a_W = 0, b_{W1} = 0.1$), we find that the likelihood function constructed with $\Delta\phi^{lV}$ does slightly better than the other two likelihood functions. We find that the BSM hypothesis for this choice of coupling strengths can be excluded at 95% confidence level with about 100fb^{-1} luminosity. For the CP violating case, ($a_W = 0, c_W = 0.1$), as expected, the two likelihood functions constructed with $\cos\delta^+$ and $\cos\delta^-$ appear to be the strongest discriminators with 95% confidence level exclusion of the BSM hypothesis is possible with about 100fb^{-1} of data. Finally for the case when ($a_W = 0, b_{W2} = 0.01$), we observe, once again, that those likelihoods constructed with $\cos\delta^+$ and $\cos\delta^-$ do slightly better than the likelihood constructed with $\Delta\phi^{lV}$. We find that 95% confidence level exclusion of this BSM hypothesis possible

⁹While it is expected that the hWW and hZZ couplings should not be too different, from a model independent approach it is important to test both couplings independently.

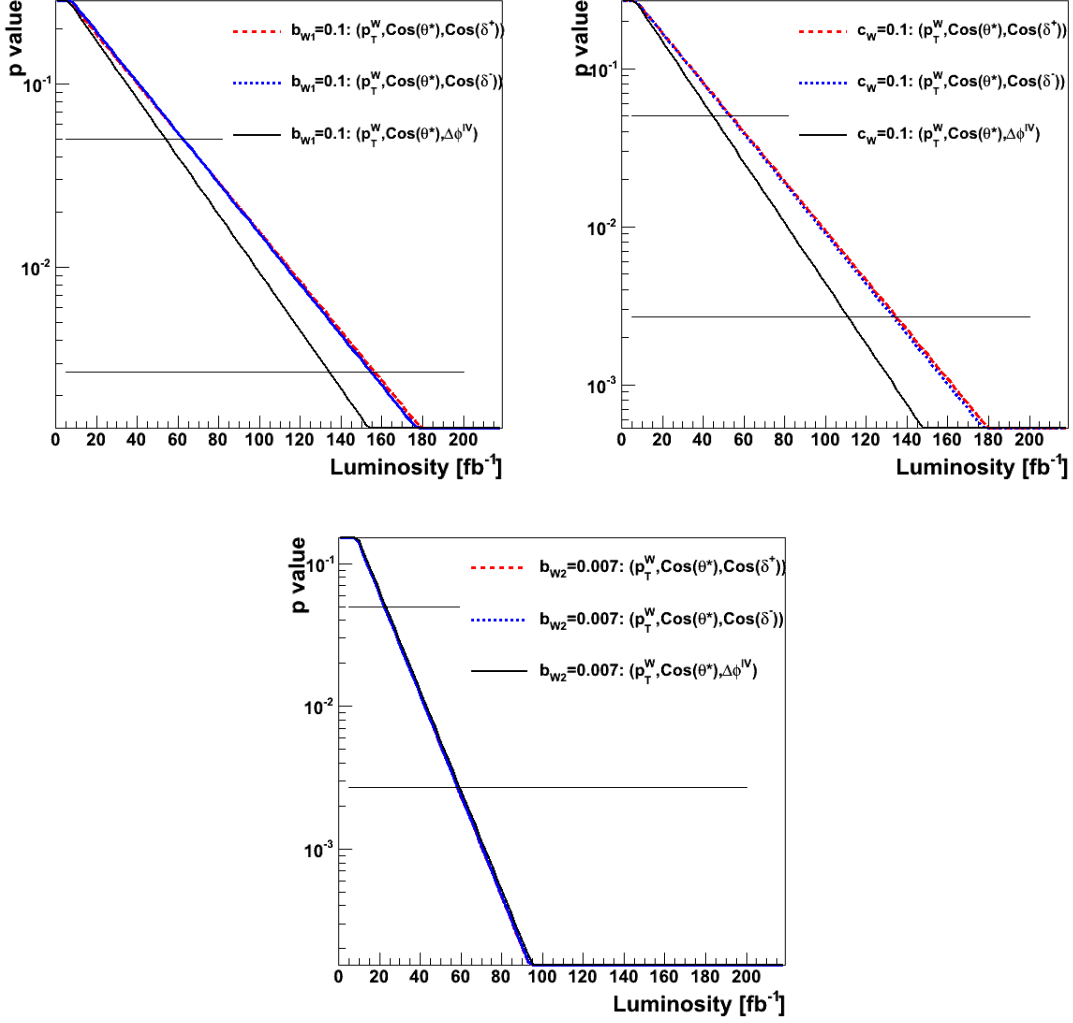


Figure 13. Plots showing the p-values for the BSM hypothesis in Wh production as a function of luminosity with three different likelihood functions: $L(p_T^W, \cos \theta^*, \cos \delta^+)$ (red-dashed), $(L(p_T^W, \cos \theta^*, \cos \delta^-))$ (blue dotted) and $(L(p_T^W, \cos \theta^*, \Delta \phi^{IV}))$ (black solid line). **Top left:** $b_{W1} = 0.1$ with all other couplings set to zero. **Top right:** $c_W = 0.1$ with all other couplings set to zero. **Bottom:** $b_{W2} = 0.007$ with all other couplings set to zero. The coupling strengths are chosen so that they reproduce the SM cross-section after applying the selection cuts. The horizontal line on top indicates exclusion of the alternate hypothesis at 95% confidence level. A second horizontal line below (if shown) indicates exclusion of the alternate hypothesis at 3 σ confidence level.

with about 50fb⁻¹ luminosity.

We also perform this analysis for Zh production. The variation of the p-value of the alternate hypothesis with luminosity for a 14 TeV LHC is shown in figure 15. Once again we compare the results of three different likelihood functions constructed out of three different combination of observables, namely $L(p_T^Z, \cos \theta^*, \cos \delta^+)$, $L(p_T^Z, \cos \theta^*, \cos \delta^-)$

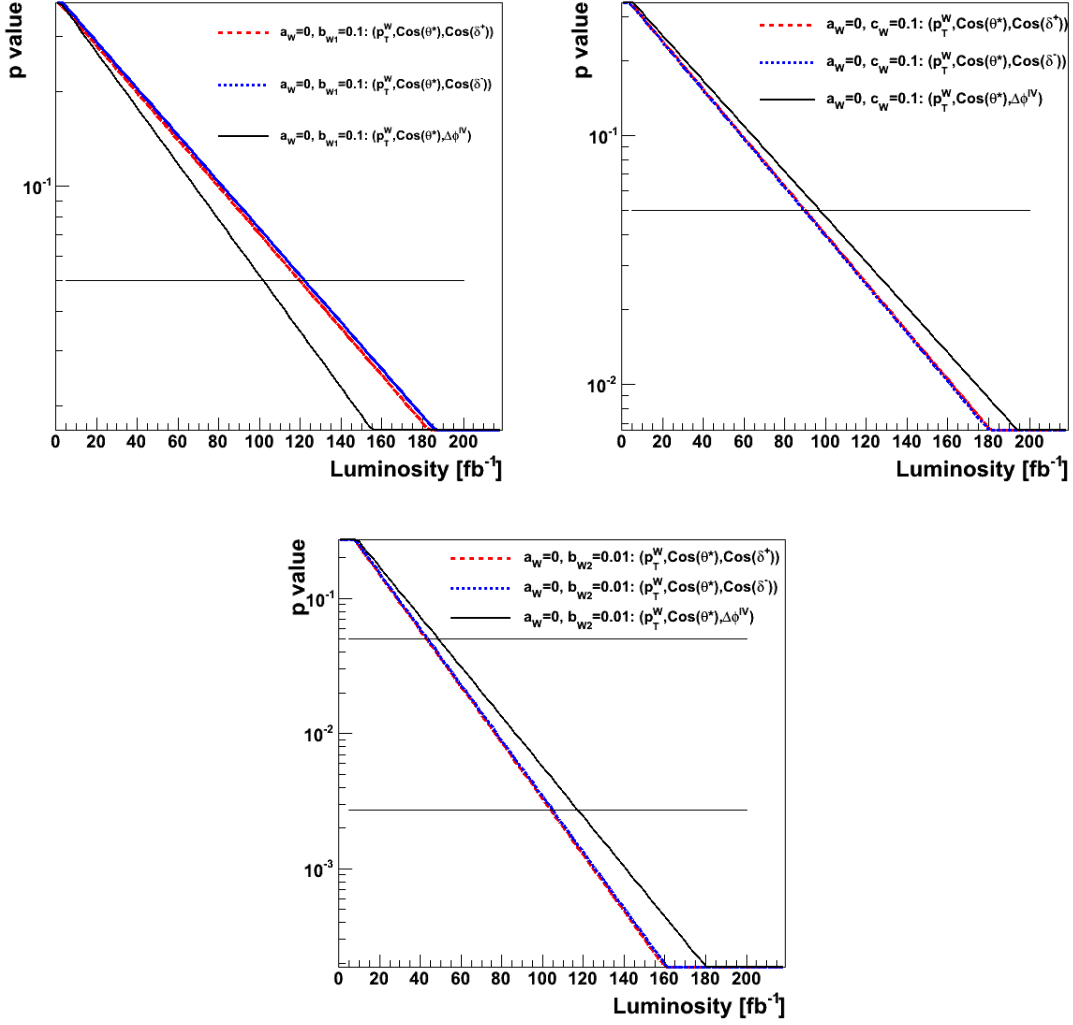


Figure 14. Plots showing the p-values for the BSM hypothesis in Wh production as a function of luminosity with three different likelihood functions: $L(p_T^W, \cos\theta^*, \cos\delta^+)$ (red-dashed), $(L(p_T^W, \cos\theta^*, \cos\delta^-))$ (blue dotted) and $(L(p_T^W, \cos\theta^*, \Delta\phi^{IV}))$ (black solid line). **Top left:** $(a_W = 0, b_{W1} = 0.1)$ with all other couplings set to zero. **Top right:** $(a_W = 0, c_W = 0.1)$ with all other couplings set to zero. **Bottom:** $(a_W = 0, b_{W2} = 0.01)$ with all other couplings set to zero. The horizontal line on top indicates exclusion of the alternate hypothesis at 95% confidence level. A second horizontal line below (if shown) indicates exclusion of the alternate hypothesis at 3 σ confidence level.

and $L(p_T^Z, \cos\theta^*, \Delta\phi^{IV})$. In contrast to Wh production we find that all three likelihoods have a discriminating power not very different from one another. The smaller cross-section for Zh production implies that the luminosities at which various hypotheses can be excluded is higher than for the corresponding hypotheses in Wh production. The luminosities at which we find exclusion of the BSM hypothesis at 95% confidence level are as follows:

- $b_{Z1} = 0.12$, with all other couplings set to zero : $\sim 100\text{fb}^{-1}$.

- $c_Z = 0.12$, with all other couplings set to zero : $\sim 90\text{fb}^{-1}$.
- $b_{Z2} = 0.019$, with all other couplings set to zero : $\sim 50\text{fb}^{-1}$.
- $(a_Z = 0, b_{Z1} = 0.1)$, with all other couplings set to zero : $\sim 100\text{fb}^{-1}$.
- $(a_Z = 0, c_Z = 0.1)$, with all other couplings set to zero : $\sim 120\text{fb}^{-1}$.
- $(a_Z = 0, b_{Z2} = 0.01)$, with all other couplings set to zero : $\sim 150\text{fb}^{-1}$.

The luminosities listed in this section are all within the projected value of 300fb^{-1} for the LHC [114]. We reiterate here that an analysis of the hVV vertex in the Vh production mode was not conceived before due to the small cross-section in this channel. We have shown that such an analysis is indeed possible. The increased acceptance to BSM physics to the cuts employed in a boosted analysis plays a crucial role in improving the sensitivity of Vh production to BSM physics. We have constructed observables that are *linearly* sensitive to BSM couplings. Further, in this section we have shown that our observables are quite powerful and exclusion of various BSM hypotheses is possible with a relatively small amount of data. The importance of our analysis is that it provides a direct method of studying the hWW vertex. As mentioned earlier, other production modes such as VBF and $h \rightarrow W^{(*)}W^*$ do not provide clean probes of the same¹⁰. It should be noted that a likelihood analysis has several nuisance parameters (from detector effects and selection cuts) that are a source of uncertainties in this analysis. In order to reduce the uncertainties in probing anomalous couplings, we look at the possibility of constructing asymmetries in the next section. This is best suited for the CP violating case where it is easy to construct asymmetries that would vanish in case of CP conservation. Note that it is possible to construct asymmetries that are non-zero for the SM and are also linear in the anomalous couplings¹¹. However, here we focus our attention on CP-violation.

5 Asymmetries

In this section, we define asymmetry parameters related to the angular observables of section 3. There are a number of motivations for this. Firstly, asymmetry parameters defined in terms of ratios are typically theoretically cleaner than kinematic distributions, due to cancellation of PDF and scale uncertainties, as well as reduced sensitivity to radiative corrections. They are also experimentally easier and cleaner to measure, being related to simple counting experiments, recording the number of events in well defined regions of phase space.

Such asymmetries can be constructed using the observables $\cos\delta^+$ and / or $\cos\delta^-$ defined in eq. (3.4). In this section we will consider the asymmetry constructed out of the

¹⁰For example, currently, CMS manages to exclude the pure pseudoscalar hypothesis at only $\sim 65\%$ CL using the WW decay channel with leptonic final states [52].

¹¹For an e^+e^- , see for example ref. [115]

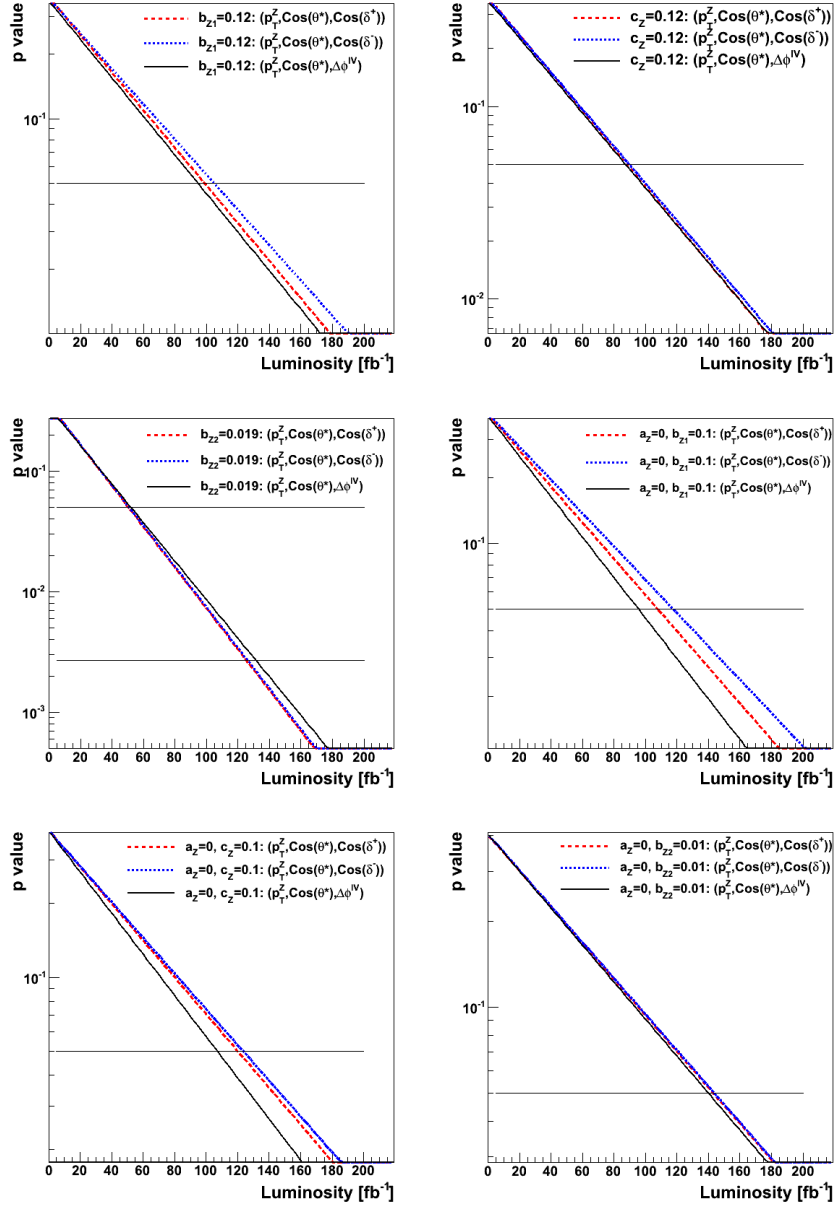


Figure 15. Plots showing the p-values for the BSM hypothesis in Zh production as a function of luminosity with three different likelihood functions: $L(p_T^Z, \cos \theta^*, \cos \delta^+)$ (red-dashed), $(L(p_T^Z, \cos \theta^*, \cos \delta^-))$ (blue dotted) and $(L(p_T^Z, \cos \theta^*, \Delta \phi^{IV}))$ (black solid line). **Top row left:** $b_{Z1} = 0.12$ with all other couplings set to zero. **Top row right:** $c_Z = 0.12$ with all other couplings set to zero. **Middle row left:** $b_{Z2} = 0.019$ with all other couplings set to zero. **Middle row right:** $(a_Z = 0, b_{Z1} = 0.1)$ with all other couplings set to zero. **Bottom row left:** $(a_Z = 0, c_Z = 0.1)$ with all other couplings set to zero. **Bottom row right:** $(a_Z = 0, b_{Z2} = 0.01)$ with all other couplings set to zero. The horizontal line on top indicates exclusion of the alternate hypothesis at 95% confidence level. A second horizontal line below (if shown) indicates exclusion of the alternate hypothesis at 3σ confidence level.

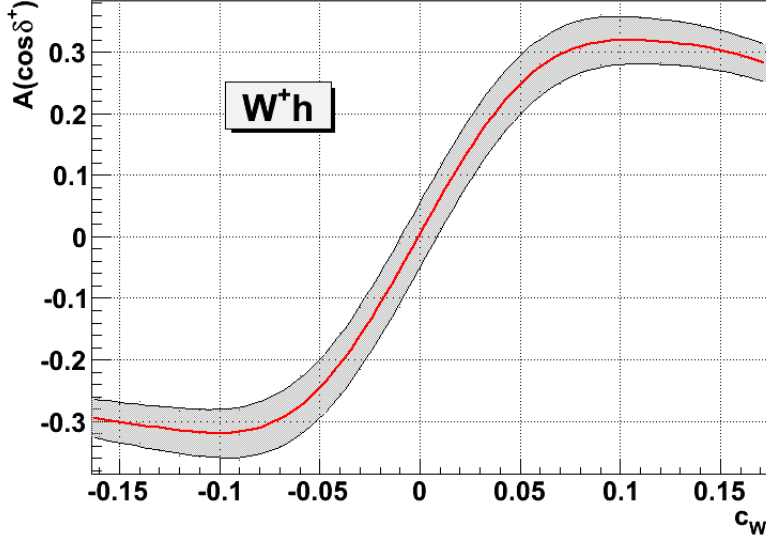


Figure 16. Variation of the asymmetry (thick red line) defined in eq. (5.1) with the strength of the coupling c_W . Here $a_W = 0$. The shaded region denotes the 1σ uncertainty in the evaluation of the asymmetry using 100 fb^{-1} of data at LHC. The asymmetry and the uncertainty have been evaluated at the parton level (as described in the text) without taking into account the effect of backgrounds.

observable $\cos \delta^+$ only¹² as follows. For W^+ events (tagged using the sign of the decay lepton) one defines

$$A(\cos \delta^+) = \frac{\sigma(\cos \delta^+ > 0) - \sigma(\cos \delta^+ < 0)}{\sigma(\cos \delta^+ > 0) + \sigma(\cos \delta^+ < 0)}, \quad (5.1)$$

defining minus this quantity for W^- events. For $(a_W = 0, c_W = 0.1)$, we find the value of this asymmetry, after applying all selection cuts, to be $A(\cos \delta^+) = 0.315$ for W^+h production. We also verify that the value of the asymmetry for all other cases (BSM, SM and backgrounds) is less than 1×10^{-3} which is within the statistical uncertainty limits of our procedure and can be safely assumed to be vanishing. We emphasize that the vanishing of this asymmetry holds true even after including detector effects. This makes it a robust observable to probe CP violation. Since the transverse momentum cuts increase the acceptance of the BSM vertex, the value of the asymmetry depends on this kinematic cut. The asymmetry also depends on rapidity cuts since the observable depends on the cross-product of the Higgs and gauge boson momenta. We perform a simple parton level analysis of W^+h production with the W^+ decaying leptonically and the Higgs decaying to a b-quark pair. In order to mimic the cuts of a boosted analysis, we apply the following cuts at the parton level:

¹²We have checked that the analogous asymmetry constructed out of the observable $\cos \delta^-$ gives similarly large values for the asymmetry. This is expected since these two observables, as described earlier, are correlated.

1. Transverse momentum of the leptons $p_T^l > 30$ GeV; rapidity $|y^l| < 2.5$; separation from b-quarks $\Delta R^{lb} > 0.3$, where $l = \{e^+, \mu^+\}$.
2. Missing transverse energy $\cancel{p}_T > 30$ GeV.
3. Transverse momentum of the b-quarks $p_T^b > 30$ GeV; rapidity $|y^b| < 2.5$; separation between b-quarks $\Delta R^{lb} > 0.1$.
4. Transverse momentum of reconstructed Higgs $p_T^h > 200$ GeV.
5. Transverse momentum of W^+ , $p_T^{W^+} > 150$ GeV and $\Delta\phi(W^+, h) > 1.2$.
6. A b-tagging efficiency of 0.6 is used and both b-jets are tagged.

We note that the value of the asymmetry calculated at the parton level is in very good agreement with the asymmetry calculated using the full boosted analysis simulation described in the previous sections ¹³. We evaluate the variation of this asymmetry with the strength of the coupling c_W using a parton level analysis. The variation of this asymmetry is shown in figure 16. We see that the sign of the asymmetry depends on the sign of c_W . We also observe that the asymmetry peaks for a value of $c_W \sim 0.1$ while a minima is observed for $c_W \sim -0.1$. The extrema signify regions where the interference plays an important role. For larger values of c_W the quadratic term (in the matrix element squared) starts contributing more strongly to the total cross-section, thus reducing the value of this asymmetry. However, this would correspond to a kinematic region where one no longer trusts the effective theory framework.

In Zh production, with $(a_Z = 1, c_Z = 0.1)$ the asymmetry is found to be ~ 0.02 , an order of magnitude less than the asymmetry in case of Wh production. The much smaller value is due to the presence of different vector and axial-vector couplings of the quarks and leptons with the Z boson, as explained earlier. Stronger probes of CP violation in the hZZ vertex can be found in ref. [116].

6 Conclusion

The ongoing attempts to pin down the nature of the recently discovered Higgs-like particle constitute a major global effort in contemporary particle physics. In this paper, we have considered the associated production of the Higgs with a massive gauge boson at the LHC as an alternative to VBF production or Higgs decays, in probing anomalous contributions to the hWW vertex. Similar analyses in VBF can be quite difficult due to large backgrounds and our inability to reconstruct the final state momenta. Furthermore, in VBF production there is a significant contribution from the hZZ vertex, reducing the ability to cleanly distinguish this from the hWW vertex. We have shown that such a separation is indeed possible in Vh production, despite the smaller cross-section. This has been made

¹³We have only tested this for three specific values of c_W .

possible with the use of modern jet-substructure techniques. Consistent with previous studies [25, 26, 109], we find that the very same selection criteria that are applied to eliminate backgrounds, also enhance the sensitivity to BSM physics. This is ultimately due to the additional momentum factors that correct the hVV vertices in an effective theory framework, which boost the Higgs to higher transverse momenta on average.

Building on the preliminary work of ref. [27], we constructed angular observables that are sensitive to new physics. To test the ability of these observables to probe the tensor structure of the hVV vertex, we performed a log likelihood analysis. Three dimensional likelihood functions were constructed with different combinations of the observables. We found that with a relatively small amount of data (less than 150fb^{-1} luminosity), it is possible to exclude all the different cases of couplings we have considered. For example we found that the CP-violating case ($a_W = 0, c_W = 0.1$) could be excluded at 95% confidence level with $\sim 90\text{fb}^{-1}$ luminosity for 14 TeV LHC.

Finally we constructed an asymmetry that is sensitive to the amount of CP violation in hWW interactions. The asymmetry vanishes for all CP-conserving cases - in particular, it is zero in the SM, such that any non-zero measurement constitutes unambiguous discovery of new physics. We checked that the asymmetry is robust against hadronization, radiation and detector effects.

The results of our paper merit further investigation, including implementation in future experimental analyses. We furthermore anticipate other useful applications that may result from combining jet substructure methods with polarisation ideas. Work in this regard is ongoing.

Acknowledgments

DJM and CDW are supported by the UK Science and Technology Facilities Council (STFC). RMG wishes to thank the Department of Science and Technology, Government of India, for support under grant no. SR/S2/JCB-64/2007. DJM and CDW thank the Indian Institute of Science for their hospitality while part of this work was carried out.

A Matrix elements for Vh production

In this appendix, we collect the matrix elements for Vh production at leading order, including the effects of the higher-dimensional operators described in section 1.

We evaluate the squared matrix element for the Feynman diagram shown in figure 17. We do not consider decay of the Higgs boson since we assume it to be spin zero and therefore its decay products will not carry information about the hWW vertex. We evaluate the matrix element squared for this process. We use the following notation to identify parts of the matrix element that are proportional to each of the anomalous couplings of eqs. (1.1,

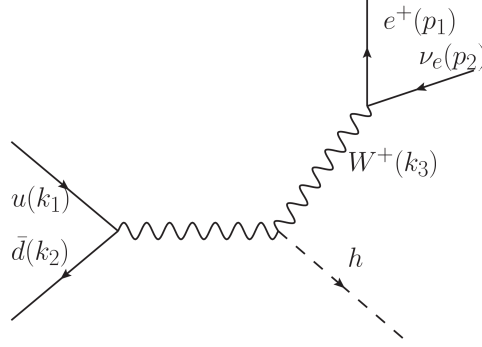


Figure 17. The Feynman diagram for the process $u\bar{d} \rightarrow W^+ h \rightarrow e^+ \nu_e h$.

1.2).

$$|\mathcal{M}_{tot}|^2 = (\mathcal{M}_{a_W} + \mathcal{M}_{b_{W1}} + \mathcal{M}_{b_{W2}} + \mathcal{M}_{c_W}) \times (\mathcal{M}_{a_W} + \mathcal{M}_{b_{W1}} + \mathcal{M}_{b_{W2}} + \mathcal{M}_{c_W})^\dagger, \quad (\text{A.1})$$

where \mathcal{M}_i , $i = \{a_W, b_{W1}, b_{W2}, c_W\}$ are the matrix elements generated from the coupling with coefficient i . In keeping with the philosophy of the effective field theory approach, we keep only terms which are at most linear in the BSM couplings (constituting the interference of the BSM physics with the SM). Quadratic terms would necessitate the inclusion also of dimension eight operators. The results are:

$$M_{a_W} = \alpha_p |\mathcal{M}_{a_W} \times \mathcal{M}_{a_W}^\dagger| = (1 + 2a_W) g_2^6 m_W^2 k_1 \cdot p_2 k_2 \cdot p_1 \quad (\text{A.2})$$

$$M_{a_W b_{W1}} = \alpha_p |\mathcal{M}_{b_{W1}} \times \mathcal{M}_{a_W}^\dagger| = \left(\frac{b_{W1}}{m_W^2} \right) g_2^6 m_W^2 (k_1 \cdot p_2 + k_2 \cdot p_1) \\ (k_1 \cdot p_2 k_2 \cdot p_1 - k_1 \cdot p_1 k_2 \cdot p_2 + k_1 \cdot k_2 p_1 \cdot p_2) \quad (\text{A.3})$$

$$M_{a_W c_W} = \alpha_p |\mathcal{M}_{c_W} \times \mathcal{M}_{a_W}^\dagger| = \left(\frac{c_W}{m_W^2} \right) g_2^6 m_W^2 \epsilon^{\{k_1, k_2, p_1, p_2\}} (k_1 \cdot p_2 + k_2 \cdot p_1) \quad (\text{A.4})$$

$$M_{a_W b_{W2}} = \alpha_p |\mathcal{M}_{a_W} \times \mathcal{M}_{b_{W2}}^\dagger| = \left(\frac{b_{W2}}{m_W^2} \right) g_2^6 m_W^2 k_1 \cdot p_2 k_2 \cdot p_1 (p_1 \cdot p_2 + k_1 \cdot k_2) \quad (\text{A.5})$$

Here $\epsilon^{\{k_1, k_2, p_1, p_2\}} = \epsilon^{\mu\nu\rho\sigma} k_{1\mu} k_{2\nu} p_{1\rho} p_{2\sigma}$ with $\epsilon^{\mu\nu\rho\sigma}$ the Levi-Civita tensor, and

$$\alpha_p = (2k_1 \cdot k_2 - m_W^2)^2 ((2p_1 \cdot p_2 - m_W^2)^2 - (m_W \Gamma_W)^2)$$

corresponds to the propagators for the W bosons. Note that the SM contribution is included in eq. (A.2).

References

- [1] **ATLAS Collaboration** Collaboration, G. Aad et al., *Observation of a new particle in the search for the Standard Model Higgs boson with the ATLAS detector at the LHC*, Phys.Lett. B716 (2012) 1–29, [[arXiv:1207.7214](#)].

- [2] **CMS Collaboration** Collaboration, S. Chatrchyan et al., *Observation of a new boson at a mass of 125 GeV with the CMS experiment at the LHC*, Phys.Lett. **B716** (2012) 30–61, [[arXiv:1207.7235](#)].
- [3] J. Espinosa, C. Grojean, M. Muhlleitner, and M. Trott, *Fingerprinting Higgs Suspects at the LHC*, JHEP **1205** (2012) 097, [[arXiv:1202.3697](#)].
- [4] J. Ellis and T. You, *Global Analysis of Experimental Constraints on a Possible Higgs-Like Particle with Mass 125 GeV*, JHEP **1206** (2012) 140, [[arXiv:1204.0464](#)].
- [5] J. Ellis and T. You, *Global Analysis of the Higgs Candidate with Mass 125 GeV*, JHEP **1209** (2012) 123, [[arXiv:1207.1693](#)].
- [6] J. R. Espinosa, M. Muhlleitner, C. Grojean, and M. Trott, *Probing for Invisible Higgs Decays with Global Fits*, JHEP **1209** (2012) 126, [[arXiv:1205.6790](#)].
- [7] T. Corbett, O. Eboli, J. Gonzalez-Fraile, and M. Gonzalez-Garcia, *Constraining anomalous Higgs interactions*, Phys.Rev. **D86** (2012) 075013, [[arXiv:1207.1344](#)].
- [8] J. Espinosa, C. Grojean, M. Muhlleitner, and M. Trott, *First Glimpses at Higgs’ face*, JHEP **1212** (2012) 045, [[arXiv:1207.1717](#)].
- [9] A. Azatov, R. Contino, and J. Galloway, *Model-Independent Bounds on a Light Higgs*, JHEP **1204** (2012) 127, [[arXiv:1202.3415](#)].
- [10] M. Montull and F. Riva, *Higgs discovery: the beginning or the end of natural EWSB?*, JHEP **1211** (2012) 018, [[arXiv:1207.1716](#)].
- [11] M. Klute, R. Lafaye, T. Plehn, M. Rauch, and D. Zerwas, *Measuring Higgs Couplings from LHC Data*, Phys.Rev.Lett. **109** (2012) 101801, [[arXiv:1205.2699](#)].
- [12] A. Azatov, R. Contino, and J. Galloway, *Contextualizing the Higgs at the LHC*, [[arXiv:1206.3171](#)].
- [13] Y. Gao, A. V. Gritsan, Z. Guo, K. Melnikov, M. Schulze, et al., *Spin determination of single-produced resonances at hadron colliders*, Phys.Rev. **D81** (2010) 075022, [[arXiv:1001.3396](#)].
- [14] S. Choi, . Miller, D.J., M. Muhlleitner, and P. Zerwas, *Identifying the Higgs spin and parity in decays to Z pairs*, Phys.Lett. **B553** (2003) 61–71, [[hep-ph/0210077](#)].
- [15] J. Ellis and D. S. Hwang, *Does the ‘Higgs’ have Spin Zero?*, JHEP **1209** (2012) 071, [[arXiv:1202.6660](#)].
- [16] A. De Rujula, J. Lykken, M. Pierini, C. Rogan, and M. Spiropulu, *Higgs look-alikes at the LHC*, Phys.Rev. **D82** (2010) 013003, [[arXiv:1001.5300](#)].
- [17] K. Odagiri, *On azimuthal spin correlations in Higgs plus jet events at LHC*, JHEP **0303** (2003) 009, [[hep-ph/0212215](#)].
- [18] C. Buszello, I. Fleck, P. Marquard, and J. van der Bij, *Prospective analysis of spin- and CP-sensitive variables in $H \rightarrow ZZ \rightarrow l(1) + l(1) - l(2) + l(2) -$ at the LHC*, Eur.Phys.J. **C32** (2004) 209–219, [[hep-ph/0212396](#)].
- [19] A. Bredenstein, A. Denner, S. Dittmaier, and M. Weber, *Precise predictions for the Higgs-boson decay $H \rightarrow WW / ZZ \rightarrow 4$ leptons*, Phys.Rev. **D74** (2006) 013004, [[hep-ph/0604011](#)].
- [20] P. Bhupal Dev, A. Djouadi, R. Godbole, M. Muhlleitner, and S. Rindani, *Determining the CP properties of the Higgs boson*, Phys.Rev.Lett. **100** (2008) 051801, [[arXiv:0707.2878](#)].

- [21] U. De Sanctis, M. Fabbrichesi, and A. Tonero, *Telling the spin of the ‘Higgs boson’ at the LHC*, Phys.Rev. **D84** (2011) 015013, [[arXiv:1103.1973](#)].
- [22] J. Ellis, V. Sanz, and T. You, *Prima Facie Evidence against Spin-Two Higgs Impostors*, Phys.Lett. **B726** (2013) 244–250, [[arXiv:1211.3068](#)].
- [23] R. Boughezal, T. J. LeCompte, and F. Petriello, *Single-variable asymmetries for measuring the ‘Higgs’ boson spin and CP properties*, [arXiv:1208.4311](#).
- [24] D. Stolarski and R. Vega-Morales, *Directly Measuring the Tensor Structure of the Scalar Coupling to Gauge Bosons*, Phys.Rev. **D86** (2012) 117504, [[arXiv:1208.4840](#)].
- [25] J. Ellis, D. S. Hwang, V. Sanz, and T. You, *A Fast Track towards the ‘Higgs’ Spin and Parity*, JHEP **1211** (2012) 134, [[arXiv:1208.6002](#)].
- [26] A. Djouadi, R. Godbole, B. Mellado, and K. Mohan, *Probing the spin-parity of the Higgs boson via jet kinematics in vector boson fusion*, Phys.Lett. **B723** (2013) 307–313, [[arXiv:1301.4965](#)].
- [27] R. Godbole, D. J. Miller, K. Mohan, and C. D. White, *Boosting Higgs CP properties via VH Production at the Large Hadron Collider*, [arXiv:1306.2573](#).
- [28] J. Ellis, V. Sanz, and T. You, *Associated Production Evidence against Higgs Impostors and Anomalous Couplings*, Eur.Phys.J. **C73** (2013) 2507, [[arXiv:1303.0208](#)].
- [29] R. Godbole, C. Hangst, M. Muhlleitner, S. Rindani, and P. Sharma, *Model-independent analysis of Higgs spin and CP properties in the process $e^+e^- \rightarrow t\bar{t}\Phi$* , Eur.Phys.J. **C71** (2011) 1681, [[arXiv:1103.5404](#)].
- [30] M. Muhlleitner, R. Godbole, C. Hangst, S. Rindani, and P. Sharma, *Analysis of Higgs spin and CP properties in a model-independent way in $e^+e^- \rightarrow t\bar{t}\Phi$* , Frascati Phys.Ser. **54** (2012) 188–197.
- [31] E. Boos, V. Bunichev, M. Dubinin, and Y. Kurihara, *Higgs boson signal at complete tree level in the SM extension by dimension-six operators*, [arXiv:1309.5410](#).
- [32] Y. Sun, X.-F. Wang, and D.-N. Gao, *CP mixed property of the Higgs-like particle in the decay channel $h \rightarrow ZZ^* \rightarrow 4l$* , [arXiv:1309.4171](#).
- [33] M. B. Einhorn and J. Wudka, *Higgs-Boson Couplings Beyond the Standard Model*, [arXiv:1308.2255](#).
- [34] I. Anderson, S. Bolognesi, F. Caola, Y. Gao, A. V. Gritsan, et al., *Constraining anomalous HVV interactions at proton and lepton colliders*, [arXiv:1309.4819](#).
- [35] E. Masso and V. Sanz, *Limits on Anomalous Couplings of the Higgs to Electroweak Gauge Bosons from LEP and LHC*, Phys.Rev. **D87** (2013), no. 3 033001, [[arXiv:1211.1320](#)].
- [36] D. T. Nhung, M. Muhlleitner, J. Streicher, and K. Walz, *Higher Order Corrections to the Trilinear Higgs Self-Couplings in the Real NMSSM*, JHEP **1311** (2013) 181, [[arXiv:1306.3926](#)].
- [37] **LHC Higgs Cross Section Working Group** Collaboration, S. Heinemeyer et al., *Handbook of LHC Higgs Cross Sections: 3. Higgs Properties*, [arXiv:1307.1347](#).
- [38] C. Delaunay, G. Perez, H. de Sandes, and W. Skiba, *Higgs Up-Down CP Asymmetry at the LHC*, Phys.Rev. **D89** (2014) 035004, [[arXiv:1308.4930](#)].
- [39] C. Delaunay, T. Golling, G. Perez, and Y. Soreq, *Charming the Higgs*, Phys.Rev. **D89** (2014) 033014, [[arXiv:1310.7029](#)].

- [40] F. Maltoni, K. Mawatari, and M. Zaro, *Higgs characterisation via vector-boson fusion and associated production: NLO and parton-shower effects*, Eur.Phys.J. **74** (2014) 2710, [[arXiv:1311.1829](#)].
- [41] H. Belusca-Maito, *Effective Higgs Lagrangian and Constraints on Higgs Couplings*, [arXiv:1404.5343](#).
- [42] M. Gavela, J. Gonzalez-Fraile, M. Gonzalez-Garcia, L. Merlo, S. Rigolin, et al., *CP violation with a dynamical Higgs*, [arXiv:1406.6367](#).
- [43] A. Biekötter, A. Knochel, M. Kraemer, D. Liu, and F. Riva, *Vices and Virtues of Higgs EFTs at Large Energy*, [arXiv:1406.7320](#).
- [44] W. Buchmüller and D. Wyler, *Effective Lagrangian Analysis of New Interactions and Flavor Conservation*, Nucl.Phys. **B268** (1986) 621.
- [45] R. Contino, M. Ghezzi, C. Grojean, M. Muhlleitner, and M. Spira, *Effective Lagrangian for a light Higgs-like scalar*, JHEP **1307** (2013) 035, [[arXiv:1303.3876](#)].
- [46] B. Grzadkowski, M. Iskrzynski, M. Misiak, and J. Rosiek, *Dimension-Six Terms in the Standard Model Lagrangian*, JHEP **1010** (2010) 085, [[arXiv:1008.4884](#)].
- [47] S. Banerjee, S. Mukhopadhyay, and B. Mukhopadhyaya, *Higher dimensional operators and LHC Higgs data : the role of modified kinematics*, Phys.Rev. **D89** (2014) 053010, [[arXiv:1308.4860](#)].
- [48] J. Ellis, V. Sanz, and T. You, *Complete Higgs Sector Constraints on Dimension-6 Operators*, JHEP **1407** (2014) 036, [[arXiv:1404.3667](#)].
- [49] N. Desai, D. K. Ghosh, and B. Mukhopadhyaya, *CP-violating HWW couplings at the Large Hadron Collider*, Phys.Rev. **D83** (2011) 113004, [[arXiv:1104.3327](#)].
- [50] S. Bolognesi, Y. Gao, A. V. Gritsan, K. Melnikov, M. Schulze, et al., *On the spin and parity of a single-produced resonance at the LHC*, Phys.Rev. **D86** (2012) 095031, [[arXiv:1208.4018](#)].
- [51] Y. Chen, A. Falkowski, I. Low, and R. Vega-Morales, *New Observables for CP Violation in Higgs Decays*, [arXiv:1405.6723](#).
- [52] **CMS Collaboration** Collaboration, S. Chatrchyan et al., *Measurement of Higgs boson production and properties in the WW decay channel with leptonic final states*, JHEP **1401** (2014) 096, [[arXiv:1312.1129](#)].
- [53] **CMS Collaboration** Collaboration, *Constraints on anomalous HVV interactions using H to 4l decays*, Tech. Rep. CMS-PAS-HIG-14-014, CERN, Geneva, 2014.
- [54] S. e. a. Dawson, *Higgs Working Group Report of the Snowmass 2013 Community Planning Study*, ArXiv e-prints (Oct., 2013) [[arXiv:1310.8361](#)].
- [55] *Measurements of the properties of the higgs-like boson in the four lepton decay channel with the atlas detector using 25 fb¹ of proton-proton collision data*, Tech. Rep. ATLAS-CONF-2013-013, CERN, Geneva, Mar, 2013.
- [56] *Properties of the higgs-like boson in the decay h to zz to 4l in pp collisions at sqrt s = 7 and 8 tev*, Tech. Rep. CMS-PAS-HIG-13-002, CERN, Geneva, 2013.
- [57] **CMS Collaboration** Collaboration, S. Chatrchyan et al., *Study of the Mass and Spin-Parity of the Higgs Boson Candidate Via Its Decays to Z Boson Pairs*, Phys.Rev.Lett. **110** (2013) 081803, [[arXiv:1212.6639](#)].

- [58] **CMS Collaboration** Collaboration, S. e. a. Chatrchyan, *Study of the mass and spin-parity of the higgs boson candidate via its decays to z boson pairs*, Phys. Rev. Lett. **110** (Feb, 2013) 081803.
- [59] **(CMS Collaboration)** Collaboration, S. e. a. Chatrchyan, *Measurement of the properties of a higgs boson in the four-lepton final state*, Phys. Rev. D **89** (May, 2014) 092007.
- [60] **D0 Collaboration** Collaboration, V. M. Abazov et al., *Constraints on spin and parity of the Higgs boson in $VH \rightarrow Vb\bar{b}$ final states*, [arXiv:1407.6369](#).
- [61] **CMS Collaboration** Collaboration, *Constraints on Anomalous HWW Interactions using Higgs boson decays to $W+W^-$ in the fully leptonic final state*, Tech. Rep. CMS-PAS-HIG-14-012, CERN, Geneva, 2014.
- [62] T. Plehn, D. L. Rainwater, and D. Zeppenfeld, *Determining the structure of Higgs couplings at the LHC*, Phys.Rev.Lett. **88** (2002) 051801, [[hep-ph/0105325](#)].
- [63] V. Hankele, G. Klamke, D. Zeppenfeld, and T. Figy, *Anomalous Higgs boson couplings in vector boson fusion at the CERN LHC*, Phys.Rev. **D74** (2006) 095001, [[hep-ph/0609075](#)].
- [64] J. R. Andersen, K. Arnold, and D. Zeppenfeld, *Azimuthal Angle Correlations for Higgs Boson plus Multi-Jet Events*, JHEP **1006** (2010) 091, [[arXiv:1001.3822](#)].
- [65] J. R. Andersen, V. Del Duca, and C. D. White, *Higgs Boson Production in Association with Multiple Hard Jets*, JHEP **0902** (2009) 015, [[arXiv:0808.3696](#)].
- [66] . Miller, D.J., S. Choi, B. Eberle, M. Muhlleitner, and P. Zerwas, *Measuring the spin of the Higgs boson*, Phys.Lett. **B505** (2001) 149–154, [[hep-ph/0102023](#)].
- [67] T. Han and J. Jiang, *CP violating $Z Z H$ coupling at $e^+ e^-$ linear colliders*, Phys.Rev. **D63** (2001) 096007, [[hep-ph/0011271](#)].
- [68] S. S. Biswal, D. Choudhury, R. M. Godbole, and Mamta, *Role of polarization in probing anomalous gauge interactions of the Higgs boson*, Phys.Rev. **D79** (2009) 035012, [[arXiv:0809.0202](#)].
- [69] S. S. Biswal and R. M. Godbole, *Use of transverse beam polarization to probe anomalous VVH interactions at a Linear Collider*, Phys.Lett. **B680** (2009) 81–87, [[arXiv:0906.5471](#)].
- [70] S. Dutta, K. Hagiwara, and Y. Matsumoto, *Measuring the Higgs-Vector boson Couplings at Linear e^+e^- Collider*, Phys.Rev. **D78** (2008) 115016, [[arXiv:0808.0477](#)].
- [71] **LHeC Study Group** Collaboration, J. Abelleira Fernandez et al., *A Large Hadron Electron Collider at CERN: Report on the Physics and Design Concepts for Machine and Detector*, J.Phys. **G39** (2012) 075001, [[arXiv:1206.2913](#)].
- [72] S. S. Biswal, R. M. Godbole, B. Mellado, and S. Raychaudhuri, *Azimuthal Angle Probe of Anomalous HWW Couplings at a High Energy ep Collider*, Phys.Rev.Lett. **109** (2012) 261801, [[arXiv:1203.6285](#)].
- [73] J. M. Butterworth, A. R. Davison, M. Rubin, and G. P. Salam, *Jet substructure as a new Higgs search channel at the LHC*, Phys.Rev.Lett. **100** (2008) 242001, [[arXiv:0802.2470](#)].
- [74] S. D. Ellis, C. K. Vermilion, and J. R. Walsh, *Techniques for improved heavy particle searches with jet substructure*, Phys.Rev. **D80** (2009) 051501, [[arXiv:0903.5081](#)].
- [75] S. D. Ellis, C. K. Vermilion, and J. R. Walsh, *Recombination Algorithms and Jet Substructure: Pruning as a Tool for Heavy Particle Searches*, Phys.Rev. **D81** (2010) 094023, [[arXiv:0912.0033](#)].

- [76] D. Krohn, J. Thaler, and L.-T. Wang, *Jet Trimming*, JHEP **1002** (2010) 084, [[arXiv:0912.1342](#)].
- [77] D. E. Soper and M. Spannowsky, *Finding physics signals with shower deconstruction*, Phys.Rev. **D84** (2011) 074002, [[arXiv:1102.3480](#)].
- [78] D. E. Soper and M. Spannowsky, *Combining subjet algorithms to enhance ZH detection at the LHC*, JHEP **1008** (2010) 029, [[arXiv:1005.0417](#)].
- [79] M. Dasgupta, A. Fregoso, S. Marzani, and G. P. Salam, *Towards an understanding of jet substructure*, JHEP **1309** (2013) 029, [[arXiv:1307.0007](#)].
- [80] M. Dasgupta, A. Fregoso, S. Marzani, and A. Powling, *Jet substructure with analytical methods*, [arXiv:1307.0013](#).
- [81] **ATLAS Collaboration** Collaboration, G. Aad et al., *Jet mass and substructure of inclusive jets in $\sqrt{s} = 7$ TeV pp collisions with the ATLAS experiment*, JHEP **1205** (2012) 128, [[arXiv:1203.4606](#)].
- [82] **ATLAS Collaboration** Collaboration, G. Aad et al., *ATLAS measurements of the properties of jets for boosted particle searches*, Phys.Rev. **D86** (2012) 072006, [[arXiv:1206.5369](#)].
- [83] **ATLAS Collaboration** Collaboration, G. Aad et al., *Performance of jet substructure techniques for large-R jets in proton-proton collisions at $\sqrt{s} = 7$ TeV using the ATLAS detector*, JHEP **1309** (2013) 076, [[arXiv:1306.4945](#)].
- [84] **CMS Collaboration** Collaboration, S. Chatrchyan et al., *Studies of jet mass in dijet and $W/Z + \text{jet}$ events*, JHEP **1305** (2013) 090, [[arXiv:1303.4811](#)].
- [85] **ATLAS Collaboration** Collaboration, G. Aad et al., *Search for resonances decaying into top-quark pairs using fully hadronic decays in pp collisions with ATLAS at $\sqrt{s} = 7$ TeV*, JHEP **1301** (2013) 116, [[arXiv:1211.2202](#)].
- [86] **ATLAS Collaboration** Collaboration, G. Aad et al., *A search for $t\bar{t}$ resonances in lepton+jets events with highly boosted top quarks collected in pp collisions at $\sqrt{s} = 7$ TeV with the ATLAS detector*, JHEP **1209** (2012) 041, [[arXiv:1207.2409](#)].
- [87] **ATLAS Collaboration** Collaboration, G. Aad et al., *Search for pair production of massive particles decaying into three quarks with the ATLAS detector in $\sqrt{s} = 7$ TeV pp collisions at the LHC*, JHEP **1212** (2012) 086, [[arXiv:1210.4813](#)].
- [88] **ATLAS Collaboration** Collaboration, G. Aad et al., *Search for pair-produced massive coloured scalars in four-jet final states with the ATLAS detector in proton-proton collisions at $\sqrt{s} = 7$ TeV*, Eur.Phys.J. **C73** (2013) 2263, [[arXiv:1210.4826](#)].
- [89] **CMS Collaboration** Collaboration, S. Chatrchyan et al., *Search for anomalous t t -bar production in the highly-boosted all-hadronic final state*, JHEP **1209** (2012) 029, [[arXiv:1204.2488](#)].
- [90] **CMS Collaboration** Collaboration, S. Chatrchyan et al., *Search for resonant $t\bar{t}$ production in lepton+jets events in pp collisions at $\sqrt{s} = 7$ TeV*, JHEP **1212** (2012) 015, [[arXiv:1209.4397](#)].
- [91] **CMS Collaboration** Collaboration, S. Chatrchyan et al., *Search for heavy resonances in the W/Z -tagged dijet mass spectrum in pp collisions at 7 TeV*, Phys.Lett. **B723** (2013) 280–301, [[arXiv:1212.1910](#)].

- [92] C. Burges and H. J. Schnitzer, *Virtual Effects of Excited Quarks as Probes of a Possible New Hadronic Mass Scale*, Nucl.Phys. **B228** (1983) 464.
- [93] C. N. Leung, S. Love, and S. Rao, *Low-Energy Manifestations of a New Interaction Scale: Operator Analysis*, Z.Phys. **C31** (1986) 433.
- [94] P. Artoisenet, P. de Aquino, F. Demartin, R. Frederix, S. Frixione, et al., *A framework for Higgs characterisation*, [arXiv:1306.6464](#).
- [95] A. Alloul, B. Fuks, and V. Sanz, *Phenomenology of the Higgs Effective Lagrangian via FeynRules*, [arXiv:1310.5150](#).
- [96] J. Alwall, M. Herquet, F. Maltoni, O. Mattelaer, and T. Stelzer, *MadGraph 5 : Going Beyond*, JHEP **1106** (2011) 128, [[arXiv:1106.0522](#)].
- [97] N. D. Christensen and C. Duhr, *FeynRules - Feynman rules made easy*, Comput.Phys.Comm. **180** (2009) 1614–1641, [[arXiv:0806.4194](#)].
- [98] A. Alloul, N. D. Christensen, C. Degrande, C. Duhr, and B. Fuks, *FeynRules 2.0 - A complete toolbox for tree-level phenomenology*, Comput.Phys.Comm. **185** (2014) 2250–2300, [[arXiv:1310.1921](#)].
- [99] T. Sjostrand, S. Mrenna, and P. Z. Skands, *PYTHIA 6.4 Physics and Manual*, JHEP **0605** (2006) 026, [[hep-ph/0603175](#)].
- [100] J. Pumplin, D. Stump, J. Huston, H. Lai, P. M. Nadolsky, et al., *New generation of parton distributions with uncertainties from global QCD analysis*, JHEP **0207** (2002) 012, [[hep-ph/0201195](#)].
- [101] M. Cacciari, G. P. Salam, and G. Soyez, *FastJet User Manual*, Eur.Phys.J. **C72** (2012) 1896, [[arXiv:1111.6097](#)].
- [102] **LHC Higgs Cross Section Working Group** Collaboration, S. Dittmaier et al., *Handbook of LHC Higgs Cross Sections: 1. Inclusive Observables*, [arXiv:1101.0593](#).
- [103] **DELPHES 3** Collaboration, J. de Favereau et al., *DELPHES 3, A modular framework for fast simulation of a generic collider experiment*, JHEP **1402** (2014) 057, [[arXiv:1307.6346](#)].
- [104] T. Han and S. Willenbrock, *QCD correction to the $pp \rightarrow WH$ and ZH total cross-sections*, Phys.Lett. **B273** (1991) 167–172.
- [105] H. Baer, B. Bailey, and J. Owens, *O (α -s) Monte Carlo approach to $W + Higgs$ associated production at hadron supercolliders*, Phys.Rev. **D47** (1993) 2730–2734.
- [106] J. Ohnemus and W. J. Stirling, *Order α -s corrections to the differential cross-section for the WH intermediate mass Higgs signal*, Phys.Rev. **D47** (1993) 2722–2729.
- [107] S. Dittmaier, S. Dittmaier, C. Mariotti, G. Passarino, R. Tanaka, et al., *Handbook of LHC Higgs Cross Sections: 2. Differential Distributions*, [arXiv:1201.3084](#).
- [108] S. Hoeche, F. Krauss, N. Lavesson, L. Lonnblad, M. Mangano, et al., *Matching parton showers and matrix elements*, [hep-ph/0602031](#).
- [109] C. Englert, M. Spannowsky, and M. Takeuchi, *Measuring Higgs CP and couplings with hadronic event shapes*, JHEP **1206** (2012) 108, [[arXiv:1203.5788](#)].
- [110] **D0** Collaboration, E. Johnson, *Spin and parity in the $WH \rightarrow \ell\nu b\bar{b}$ channel at the D0 experiment*, [arXiv:1305.3675](#).

- [111] T. Han and Y. Li, *Genuine CP-odd Observables at the LHC*, Phys.Lett. **B683** (2010) 278–281, [[arXiv:0911.2933](#)].
- [112] N. D. Christensen, T. Han, and Y. Li, *Testing CP Violation in ZZH Interactions at the LHC*, Phys.Lett. **B693** (2010) 28–35, [[arXiv:1005.5393](#)].
- [113] C. Englert, D. Goncalves-Netto, K. Mawatari, and T. Plehn, *Higgs Quantum Numbers in Weak Boson Fusion*, JHEP **1301** (2013) 148, [[arXiv:1212.0843](#)].
- [114] **CMS Collaboration** Collaboration, *Projected Performance of an Upgraded CMS Detector at the LHC and HL-LHC: Contribution to the Snowmass Process*, [arXiv:1307.7135](#).
- [115] S. S. Biswal, R. M. Godbole, R. K. Singh, and D. Choudhury, *Signatures of anomalous VVH interactions at a linear collider*, Phys.Rev. **D73** (2006) 035001, [[hep-ph/0509070](#)].
- [116] R. M. Godbole, D. Miller, and M. M. Muhlleitner, *Aspects of CP violation in the H ZZ coupling at the LHC*, JHEP **0712** (2007) 031, [[arXiv:0708.0458](#)].